Composite Structures 95 (2013) 676–690

Contents lists available at SciVerse ScienceDirect

Composite Structures

journal homepage: www.elsevier.com/locate/compstruct

A thermo-mechanical analysis of functionally graded beams via hierarchical modelling

G. Giunta [a,*], D. Crisafulli [a,b], S. Belouettar [a], E. Carrera [b]

[a] Centre de Recherche Public Henri Tudor, 29, Av. John F. Kennedy, L-1855 Luxembourg-Kirchberg, Luxembourg
[b] Politecnico di Torino, 24, c.so Duca degli Abruzzi, 10129 Turin, Italy

ARTICLE INFO

Article history:
Available online 17 August 2012

Keywords:
Thermal loads
Beam structures
Functionally graded materials
Unified formulation
Closed form solution

ABSTRACT

In this work, functionally graded beams subjected to thermal loadings are analysed. To this end, several beam models are hierarchically derived by means of a unified formulation that makes the formulation independent from the displacements polynomial approximation order over the cross-section. The temperature profile is determined by solving Fourier's heat conduction equation. The governing equations are, then, derived from the Principle of Virtual Displacements considering the temperature field as an external load. A Navier-type, closed form solution is used. Simply supported beams are, therefore, considered. Functionally graded mono-layer and sandwich cross-section configurations are investigated. Numerical results in terms of temperature, displacement and stress distributions are provided for different beam slenderness ratios. Results are assessed towards three-dimensional finite element solutions demonstrating that accurate results can be obtained with reduced computational costs.

1. Introduction

Beam-like structures operating in severe temperature environments are examples of typical aeronautical and space applications. High-temperature resistant materials are, therefore, required. Structures made of ceramic–metal Functionally Graded Materials (FGMs) are able to combine temperature resistance and a continuous stress distribution because of a smooth variation of material properties along some preferred directions.

A brief overview of recent works about thermo-mechanical analysis of functionally graded structures is presented below. Several applications of the theory of thermo-elasticity can be found in the book by Hetnarski and Eslami [1]. In particular, the thermal stress analysis of beams based on Euler–Bernoulli assumptions was presented. Beams made of functionally graded materials were also investigated. The problem of thermal stresses in FGMs was addressed by Noda [2]. The optimal gradation profiles to decrease the thermal stresses in FGMs were discussed. The thermoelastic behaviour of functionally graded beams was also studied by Chakraborty et al. [3]. A beam finite element based on Timoshenko's theory was developed, accounting for an exponential and a power law through-the-thickness variation of elastic and thermal properties. A thermo-elastic stress analysis of multi-layered non-homogeneous beams was carried out by Carpinteri and Paggi [4]. Analytical solutions were provided under Euler–Bernoulli's kinematic hypotheses. Functionally graded materials were also investigated, considering a linear variation of material properties along the beam's thickness. A meshless method for thermo-elastic analysis of functionally graded materials combined with radial basis functions was presented by Wang and Qin [5]. Mahi et al. [6] studied the free vibration of FGM beams subjected to initial thermal stress. Exact solutions based on several shear deformation theories were presented considering different boundary conditions. The temperature profile was computed solving a one-dimensional steady-state heat conduction equation. Thermal buckling and thermo-elastic vibration analysis of FGM beams were carried out by Wattanasakulpong et al. [7] by means of a third-order shear deformation theory. Material properties were considered to dependent on the temperature via a non-linear polynomial law [8]. The static response of functionally graded plates subjected to thermal loads was addressed by Brischetto et al. [9]. The temperature field was determined by solving Fourier's equation. Different volume fractions of the material constituents were considered to evaluate the temperature, displacement and stress distributions.

A thermal analysis of functionally graded beams via refined models is addressed in this paper. Models are derived via a Unified Formulation (UF) that has been previously proposed for plates and shells (see Carrera [10]) and extended to solid and composite beams (see Carrera et al. [11], Giunta et al. [12,13] and Catapano et al. [14]). In the proposed UF, the displacements' polynomial

* Corresponding author. Address: Department of Advanced Materials and Structures, Centre de Recherche Public Henri Tudor, 29, Av. John F. Kennedy, L-1855 Luxembourg-Kirchberg, Luxembourg. Tel.: +352 54 55 80 479; fax: +352 42 59 91 555.
E-mail address: gaetano.giunta@tudor.lu (G. Giunta).

0263-8223/$ - see front matter © 2012 Elsevier Ltd. All rights reserved.
http://dx.doi.org/10.1016/j.compstruct.2012.08.013

approximation over the beam cross-section is derived in a compact form. The governing equations variationally consistent with the assumed kinematic hypothesis are derived through the Principle of Virtual Displacement (PVD) in terms of a fundamental nucleo. This nucleo does not depend upon the displacements order of expansion. As a result, a set of several kinematic models can be obtained that accounts for transverse shear deformations and cross-section in- and out-of-plane warping. The temperature field is obtained by solving Fourier's heat conduction equation. Governing differential equations are solved via a Navier-type, closed form solution. Slender and deep beams are investigated. As far as the material gradation along the beam cross-section is concerned, the material gradation is considered by means of a Lagrange approximation based upon a Newton series expansion upon a Chebyshev grid of sampling points over the cross-section. In such a manner, the fundamental nucleo is formulated in a general manner with respect to the particular gradation law. The numerical investigations are carried out considering a power law variation along the beam thickness direction of the elastic and thermal material properties. The proposed models are validated through comparison with three-dimensional FEM solutions. Numerical results show that accurate results can be obtained with small computational costs.

2. Preliminaries

A beam, see Fig. 1, is a structure whose axial extension (l) is predominant if compared to any other dimension orthogonal to it. The cross-section (Ω) is identified by intersecting the beam with planes that are orthogonal to its axis. A Cartesian reference system is adopted: y- and z-axis are two orthogonal directions laying on Ω. The x coordinate is coincident to the axis of the beam. It is bounded such that $0 \leqslant x \leqslant l$. The cross-section is considered to be constant along x. The displacement field is:

$$\mathbf{u}^T(x,y,z) = \{\, u_x(x,y,z) \quad u_y(x,y,z) \quad u_z(x,y,z) \,\} \tag{1}$$

in which u_x, u_y and u_z are the displacement components along x-, y- and z-axis. Superscript 'T' represents the transposition operator. Stress, $\boldsymbol{\sigma}$, and strain, $\boldsymbol{\varepsilon}$, vectors are grouped into vectors $\boldsymbol{\sigma}_n$, $\boldsymbol{\varepsilon}_n$ that lay on the cross-section:

$$\boldsymbol{\sigma}_n^T = \{\, \sigma_{xx} \quad \sigma_{xy} \quad \sigma_{xz} \,\} \quad \boldsymbol{\varepsilon}_n^T = \{\, \varepsilon_{xx} \quad \varepsilon_{xy} \quad \varepsilon_{xz} \,\} \tag{2}$$

and $\boldsymbol{\sigma}_p$, $\boldsymbol{\varepsilon}_p$ laying on planes orthogonal to Ω:

$$\boldsymbol{\sigma}_p^T = \{\, \sigma_{yy} \quad \sigma_{zz} \quad \sigma_{yz} \,\} \quad \boldsymbol{\varepsilon}_p^T = \{\, \varepsilon_{yy} \quad \varepsilon_{zz} \quad \varepsilon_{yz} \,\} \tag{3}$$

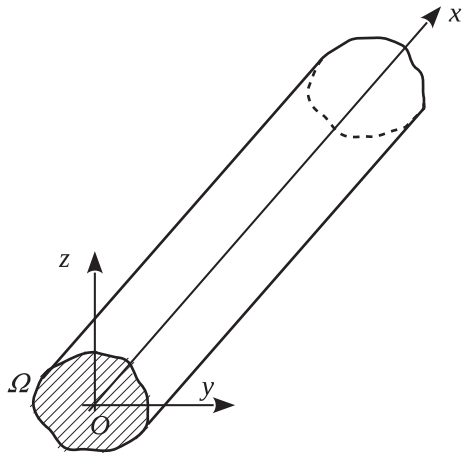

Fig. 1. Beam structure and reference system.

Table 1
Mac Laurin's polynomials terms via Pascal's triangle.

N	N_u	F_τ
0	1	$F_1 = 1$
1	3	$F_2 = y$ $F_3 = z$
2	6	$F_4 = y^2$ $F_5 = yz$ $F_6 = z^2$
3	10	$F_7 = y^3$ $F_8 = y^2 z$ $F_9 = yz^2$ $F_{10} = z^3$
...	...	...
N	$\frac{(N+1)(N+2)}{2}$	$F_{\frac{(N^2+N+2)}{2}} = y^N$ $F_{\frac{(N^2+N+4)}{2}} = y^{N-1}z$ $\cdots$ $F_{\frac{N(N+3)}{2}} = yz^{N-1}$ $F_{\frac{(N+1)(N+2)}{2}} = z^N$

Table 2
FGM constituents elastic and thermal properties.

	E (GPa)	ν	K (W/mK)	α (10^{-6} K^{-1})
Zirconia	151.01	0.300	2.09	10.
Monel	179.40	0.368	25.00	15.

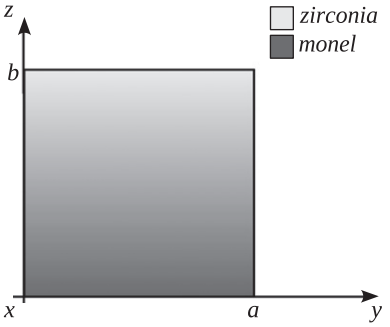

Fig. 2. Mono-layer FGM beam.

Under the hypothesis of linear analysis, the following strain–displacement geometrical relations hold:

$$\begin{aligned} \boldsymbol{\varepsilon}_n^T &= \{\, u_{x,x} \quad u_{x,y} + u_{y,x} \quad u_{x,z} + u_{z,x} \,\} \\ \boldsymbol{\varepsilon}_p^T &= \{\, u_{y,y} \quad u_{z,z} \quad u_{y,z} + u_{z,y} \,\} \end{aligned} \tag{4}$$

Subscripts 'x', 'y' and 'z', when preceded by comma, represent derivation versus the corresponding spatial coordinate. A compact vectorial notation can be adopted for Eq. (4):

$$\begin{aligned} \boldsymbol{\varepsilon}_n &= \mathbf{D}_{np}\mathbf{u} + \mathbf{D}_{nx}\mathbf{u} \\ \boldsymbol{\varepsilon}_p &= \mathbf{D}_p\mathbf{u} \end{aligned} \tag{5}$$

where $\mathbf{D}_{np}$, $\mathbf{D}_{nx}$ and $\mathbf{D}_p$ are the following differential matrix operators:

$$\mathbf{D}_{np} = \begin{bmatrix} 0 & 0 & 0 \\ \frac{\partial}{\partial y} & 0 & 0 \\ \frac{\partial}{\partial z} & 0 & 0 \end{bmatrix} \quad \mathbf{D}_{nx} = \mathbf{I}\frac{\partial}{\partial x} \quad \mathbf{D}_p = \begin{bmatrix} 0 & \frac{\partial}{\partial y} & 0 \\ 0 & 0 & \frac{\partial}{\partial z} \\ 0 & \frac{\partial}{\partial z} & \frac{\partial}{\partial y} \end{bmatrix} \tag{6}$$

$\mathbf{I}$ is the unit matrix. In the case of thermo-mechanical problems, the constitutive equations are:

$$\begin{aligned} \boldsymbol{\sigma}_p &= \boldsymbol{\sigma}_{pe} - \boldsymbol{\sigma}_{pt} = \mathbf{C}_{pp}\boldsymbol{\varepsilon}_p + \mathbf{C}_{pn}\boldsymbol{\varepsilon}_n - \lambda_p T \\ \boldsymbol{\sigma}_n &= \boldsymbol{\sigma}_{ne} - \boldsymbol{\sigma}_{nt} = \mathbf{C}_{np}\boldsymbol{\varepsilon}_p + \mathbf{C}_{nn}\boldsymbol{\varepsilon}_n - \lambda_n T \end{aligned} \tag{7}$$

where subscripts 'e' and 't' refer to the elastic and the thermal contributions, respectively. For isotropic materials, the matrices $\mathbf{C}_{pp}$, $\mathbf{C}_{pn}$, $\mathbf{C}_{np}$ and $\mathbf{C}_{nn}$ in Eq. (7) are:

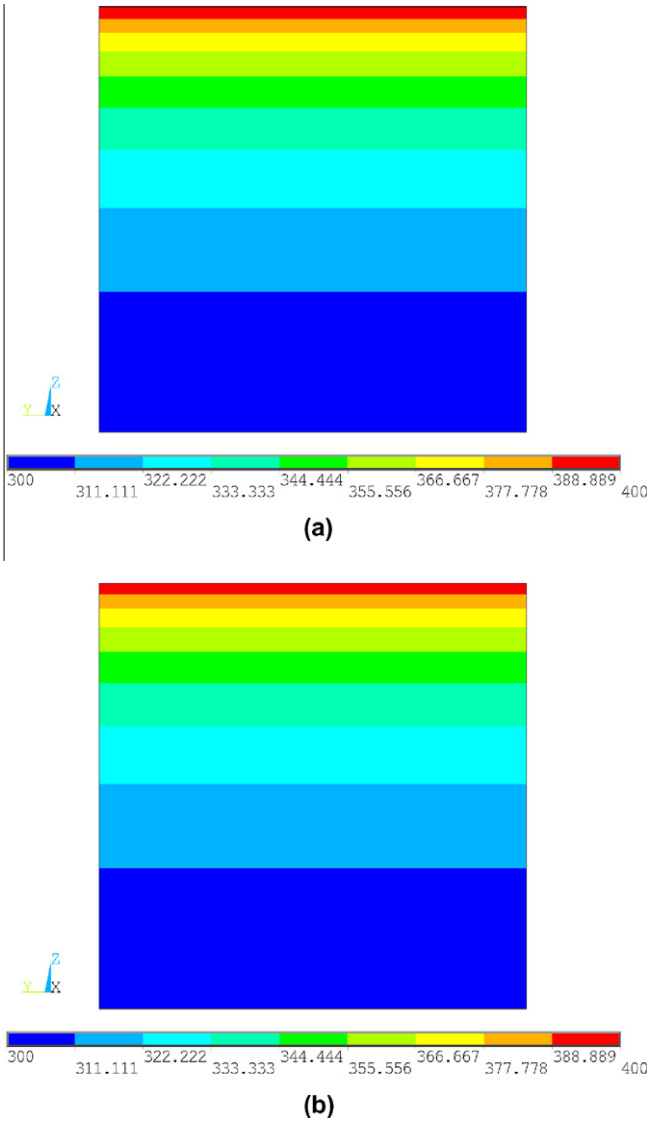

Fig. 3. Mono-layer FGM beam temperature profile [K] at $x/l = 1/2$ via (a) Fourier's equation solution and (b) FEM 3D[a], $l/a = 10$.

$$\mathbf{C}_{pp} = \begin{bmatrix} C_{22} & C_{23} & 0 \\ C_{23} & C_{33} & 0 \\ 0 & 0 & C_{44} \end{bmatrix} \quad \mathbf{C}_{pn} = \mathbf{C}_{np}^T = \begin{bmatrix} C_{12} & 0 & 0 \\ C_{13} & 0 & 0 \\ 0 & 0 & 0 \end{bmatrix}$$
$$\mathbf{C}_{nn} = \begin{bmatrix} C_{11} & 0 & 0 \\ 0 & C_{66} & 0 \\ 0 & 0 & C_{55} \end{bmatrix} \tag{8}$$

The coefficients C_{ij} are:

$$C_{11} = C_{22} = C_{33} = \frac{1-\nu}{(1+\nu)(1-2\nu)}E$$
$$C_{12} = C_{13} = C_{23} = \frac{\nu}{(1+\nu)(1-2\nu)}E$$
$$C_{44} = C_{55} = C_{66} = \frac{1}{2(1+\nu)}E \tag{9}$$

being Young's modulus (E) and Poisson's ratio (ν) function of the cross-section coordinates. The coefficients λ_n and λ_p:

$$\boldsymbol{\lambda}_n^T = \{\lambda_1 \quad 0 \quad 0\} \quad \boldsymbol{\lambda}_p^T = \{\lambda_2 \quad \lambda_3 \quad 0\} \tag{10}$$

are related to the thermal expansion coefficients α_n and α_p:

Table 3
Mono-layer FGM beam, displacements (m), $l/a = 100$.

	$-10 \cdot \bar{u}_z$	$-10 \cdot \bar{u}_x$	$10^3 \cdot \bar{u}_y$
FEM 3D[a]	6.583	1.204	1.972
FEM 3D[b]	6.527	1.205	1.967
$N = 9 - 13$	6.533	1.205	1.961
$N = 8$	6.533	1.205	1.960
$N = 7$	6.533	1.205	1.958
$N = 6$	6.534	1.205	1.955
$N = 5$	6.534	1.205	1.950
$N = 4$	6.538	1.205	1.948
$N = 3$	6.537	1.205	1.937
$N = 2$	6.697	1.202	1.889
TBT	6.522	1.205	0.000
EBT	6.521	1.205	0.000

[a] Mesh $30 \times 30 \times 30$.
[b] Mesh $20 \times 20 \times 20$.

Table 4
Mono-layer FGM beam, stresses (Pa), $l/a = 100$.

	$10^{-7} \cdot \bar{\sigma}_{xx}$	$10^{-5} \cdot \bar{\sigma}_{xz}$	$10^{-6} \cdot \bar{\sigma}_{zz}$
FEM 3D[a]	1.088	2.247	5.522
FEM 3D[b]	1.098	2.239	5.590
$N = 13$	1.109	2.232	5.582
$N = 12$	1.119	2.235	5.778
$N = 11$	1.119	2.240	5.770
$N = 10$	1.121	2.231	5.804
$N = 9$	1.120	2.225	5.800
$N = 8$	1.115	2.218	5.736
$N = 7$	1.117	2.191	5.772
$N = 6$	1.171	2.293	6.618
$N = 5$	1.156	2.289	6.333
$N = 4$	0.885	1.892	1.516
$N = 3$	0.945	2.020	2.451
$N = 2$	2.351	1.573	23.55
TBT	0.793	4.135[c]	–[d]
EBT	0.787	–	–

[a] Mesh $30 \times 30 \times 30$.
[b] Mesh $20 \times 20 \times 20$.
[c] Scaling factor -10^5 (instead of 10^{-5}).
[d] Result not provided by the theory.

Table 5
Mono-layer FGM beam, displacements (m), $l/a = 10$.

	$-10^3 \cdot u_z$	$-10^2 \cdot u_x$	$10^3 \cdot u_y$
FEM 3D[a]	6.704	1.195	1.953
FEM 3D[b]	6.644	1.196	1.958
$N = 12,13$	6.648	1.197	1.955
$N = 9–11$	6.648	1.197	1.954
$N = 8$	6.648	1.197	1.953
$N = 7$	6.648	1.197	1.952
$N = 6$	6.648	1.197	1.947
$N = 5$	6.648	1.197	1.943
$N = 4$	6.653	1.197	1.940
$N = 3$	6.655	1.197	1.929
$N = 2$	6.854	1.194	1.866
TBT	6.649	1.191	0.000
EBT	6.648	1.191	0.000

[a] Mesh $30 \times 30 \times 30$.
[b] Mesh $20 \times 20 \times 20$.

$$\boldsymbol{\alpha}_n^T = \{\alpha_1 \quad 0 \quad 0\} \quad \boldsymbol{\alpha}_p^T = \{\alpha_2 \quad \alpha_3 \quad 0\} \tag{11}$$

through the following equations:

$$\boldsymbol{\lambda}_p = \mathbf{C}_{pp}\boldsymbol{\alpha}_p + \mathbf{C}_{pn}\boldsymbol{\alpha}_n$$
$$\boldsymbol{\lambda}_n = \mathbf{C}_{np}\boldsymbol{\alpha}_p + \mathbf{C}_{nn}\boldsymbol{\alpha}_n \tag{12}$$

A Lagrange approximation on N_p Chebyshev points along y and z cross-section co-ordinates based on Newton series expansion is assumed for the material stiffness coefficients C_{ij} and thermal coefficients λ_i:

$$\begin{aligned} C_{ij}(y,z) &\approx \omega_\xi(y)\omega_\eta(z)C_{ij}[y_0,y_1,\ldots,y_\xi;\ z_0,z_1,\ldots,z_\eta] \\ \lambda_i(y,z) &\approx \omega_\xi(y)\omega_\eta(z)\lambda_i[y_0,y_1,\ldots,y_\xi;\ z_0,z_1,\ldots,z_\eta] \\ &\text{with } \xi,\eta = 0,1,\ldots,N_p \end{aligned} \tag{13}$$

being:

$$\omega_m(\zeta) = \begin{cases} 1 & m = 0 \\ \prod_{n=0}^{m-1}(\zeta - \zeta_n) & m \in [1,N_p] \end{cases} \tag{14}$$

and $C_{ij}[\ldots;\ldots]$ and $\lambda_i[\ldots;\ldots]$ the divided difference of the approximated function, see Philips [15]. Chebyshev's points are defined on the domain [−1,+1] via the following equation:

$$\zeta_m = \cos\left(\frac{m\pi}{N_p}\right) \quad \text{with } m = 0,1,\ldots,N_p \tag{15}$$

These points are then mapped into the cross-section domain via a variable transformation. In this manner, the software implementation of the proposed models is general and does not depend upon a specific gradation law that, once defined, will be approximated via a Newton series expansion.

The beam models are derived considering the temperature (T) as an external loading resulting from the internal thermal stresses. This requires that the temperature profile is known over the whole beam domain. Fourier's heat conduction equation is solved in order to obtain T. In order to obtain a strong form solution of the problem governing equations, the temperature is written as follows:

$$T(x,y,z) = \Theta_n(x)\Theta_\Omega(y,z) \tag{16}$$

The whole solution procedure is presented in Appendix A.

3. Hierarchical beam theories

The variation of the displacement field over the cross-section can be postulated a priori. Several displacement-based theories can be formulated on the basis of the following generic kinematic field:

$$\mathbf{u}(x,y,z) = F_\tau(y,z)\mathbf{u}_\tau(x) \quad \text{with } \tau = 1,2,\ldots,N_u \tag{17}$$

where N_u stands for the number of unknowns. It depends on the approximation order N that is a free parameter of the formulation. The compact expression is based on Einstein's notation: a repeated index stands for summation. Thanks to this notation, problem's governing differential equations and boundary conditions can be derived in terms of a single 'fundamental nucleo'. The complexity related to higher than classical approximation terms is tackled and the theoretical formulation is valid for the generic approximation order and approximating functions $F_\tau(y,z)$. In this paper, the functions F_τ are assumed to be Mac Laurin's polynomials. This choice is inspired by the classical beam models. N_u and F_τ as functions of N can be obtained via Pascal's triangle as shown in Table 1. The actual governing differential equations and boundary conditions due to a fixed approximation order and polynomials type are obtained straightforwardly via summation of the nucleo corresponding to each term of the expansion. According to the previous choice of the polynomial functions, the generic, N-order displacement field is:

$$\begin{aligned} u_x &= u_{x1} + u_{x2}y + u_{x3}z + \cdots + u_{x\frac{(N^2+N+2)}{2}}y^N + \cdots + u_{x\frac{(N+1)(N+2)}{2}}z^N \\ u_y &= u_{y1} + u_{y2}y + u_{y3}z + \cdots + u_{y\frac{(N^2+N+2)}{2}}y^N + \cdots + u_{y\frac{(N+1)(N+2)}{2}}z^N \\ u_z &= u_{z1} + u_{z2}y + u_{z3}z + \cdots + u_{z\frac{(N^2+N+2)}{2}}y^N + \cdots + u_{z\frac{(N+1)(N+2)}{2}}z^N \end{aligned} \tag{18}$$

Table 6
Mono-layer FGM beam, stresses (Pa), $l/a = 10$.

	$10^{-6}\cdot\bar{\sigma}_{xx}$	$10^{-6}\cdot\bar{\sigma}_{xz}$	$10^{-6}\cdot\bar{\sigma}_{zz}$
FEM 3D[a]	8.635	2.292	6.459
FEM 3D[b]	8.738	2.284	6.535
$N = 13$	8.865	2.276	6.521
$N = 12$	8.968	2.279	6.722
$N = 11$	8.964	2.285	6.714
$N = 10$	8.980	2.276	6.740
$N = 9$	8.977	2.270	6.735
$N = 8$	8.915	2.261	6.663
$N = 7$	8.942	2.232	6.703
$N = 6$	9.540	2.335	7.648
$N = 5$	9.374	2.331	7.330
$N = 4$	6.383	1.925	2.011
$N = 3$	7.024	2.058	3.020
$N = 2$	23.19	1.601	27.53
TBT	10.62	4.090[c]	–[d]
EBT	10.57	–	–

[a] Mesh 30 × 30 × 30.
[b] Mesh 20 × 20 × 20.
[c] Scaling factor -10^5 (instead of 10^{-6}).
[d] Result not provided by the theory.

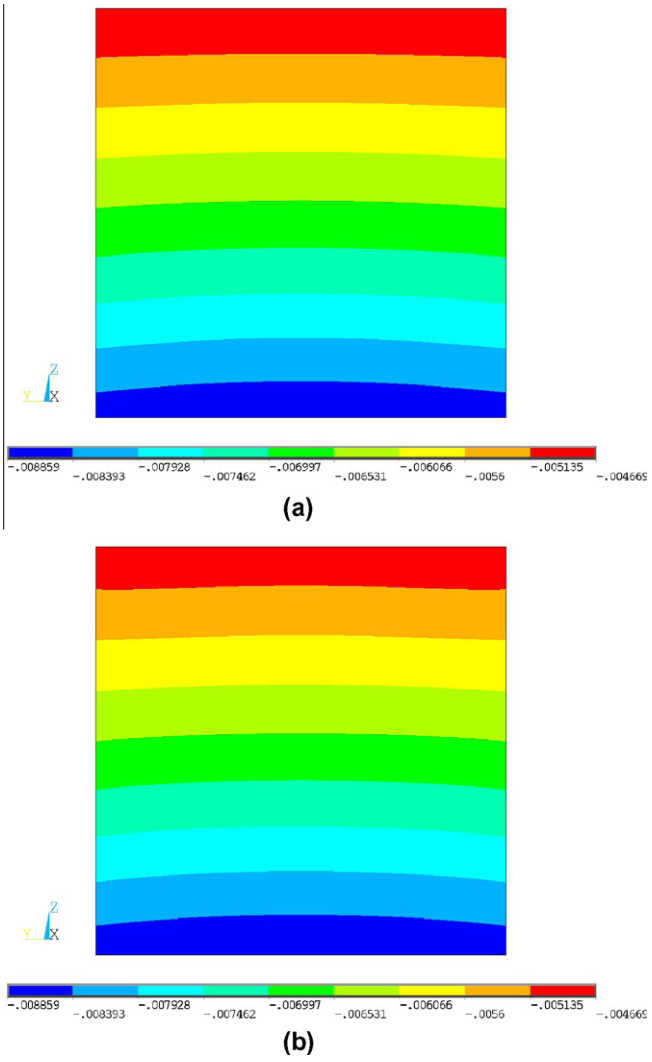

Fig. 4. Mono-layer FGM beam, u_z [m] at $x/l = 1/2$ via (a) $N = 4$ and (b) FEM 3D[a], $l/a = 10$.

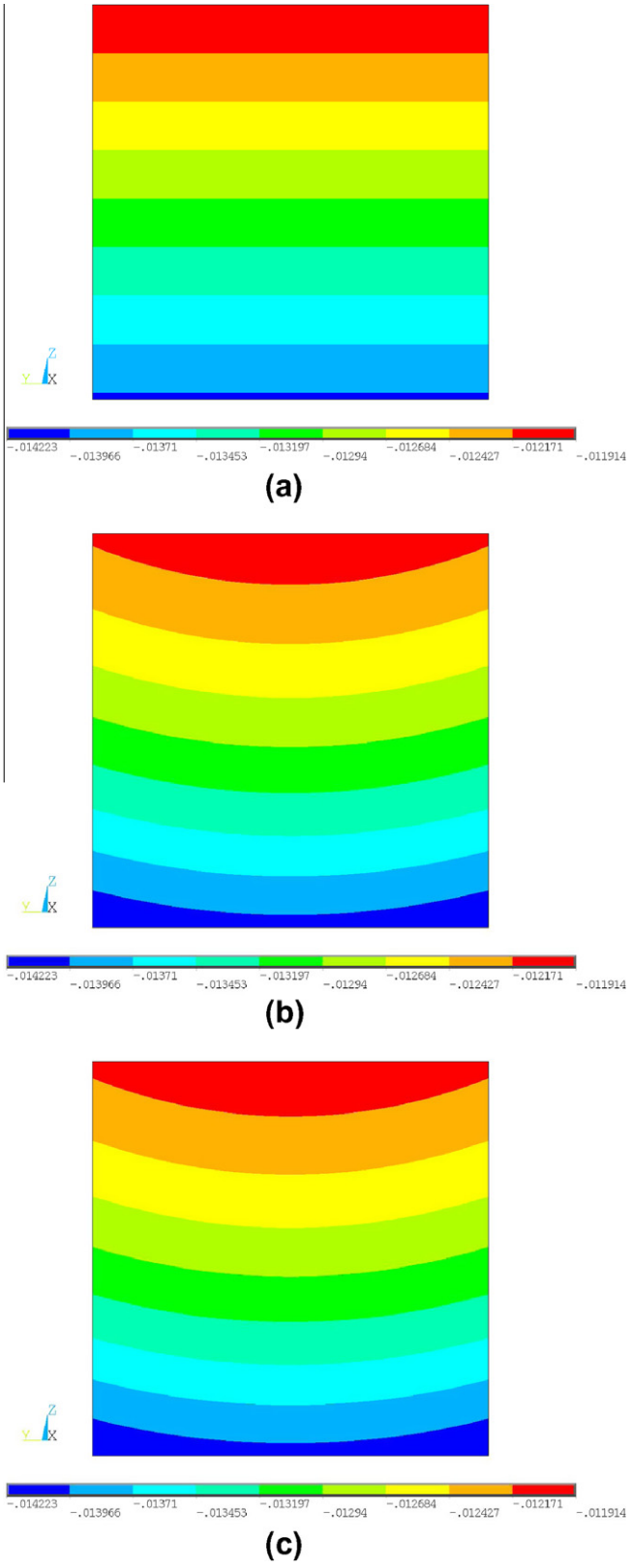

Fig. 5. Mono-layer FGM beam, u_x [m] at $x/l = 0$ via (a) TBT, (b) $N = 4$ and (c) FEM 3D[a], $l/a = 10$.

As far as the first-order approximation order is concerned, the kinematic field is:

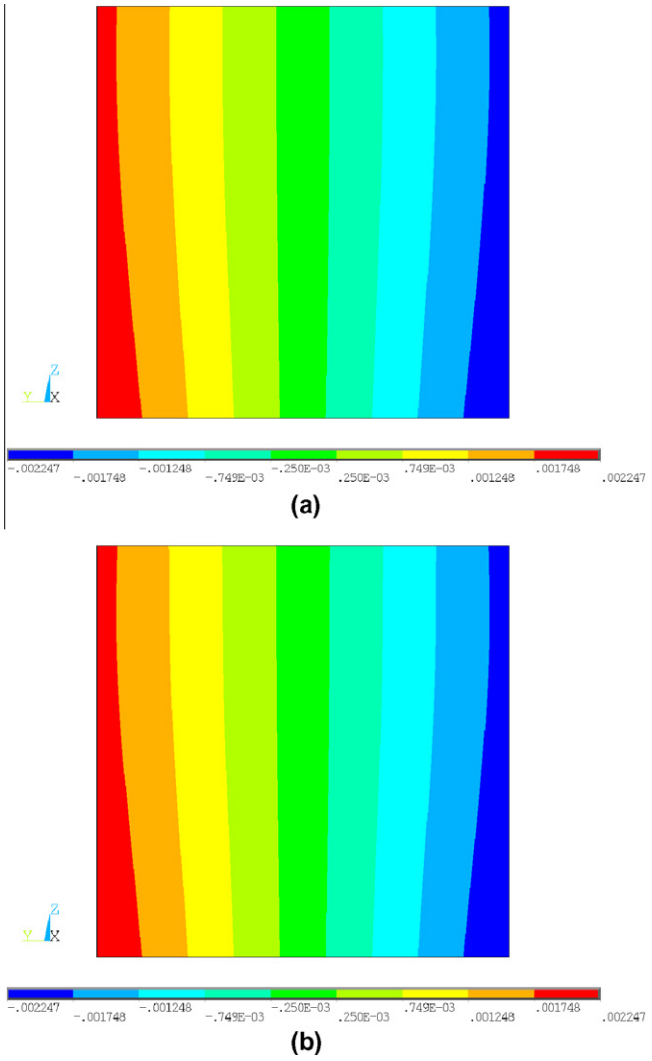

Fig. 6. Mono-layer FGM beam, u_y [m] at $x/l = 1/2$ via (a) $N = 4$ and (b) FEM 3D[a], $l/a = 10$.

$$\begin{aligned} u_x &= u_{x1} + u_{x2}y + u_{x3}z \\ u_y &= u_{y1} + u_{y2}y + u_{y3}z \\ u_z &= u_{z1} + u_{z2}y + u_{z3}z \end{aligned} \tag{19}$$

Classical models, such as Timoshenko beam theory (TBT):

$$\begin{aligned} u_x &= u_{x1} + u_{x2}y + u_{x3}z \\ u_y &= u_{y1} \\ u_z &= u_{z1} \end{aligned} \tag{20}$$

and Euler–Bernoulli beam theory (EBT):

$$\begin{aligned} u_x &= u_{x1} - u_{y1,x}y - u_{z1,x}z \\ u_y &= u_{y1} \\ u_z &= u_{z1} \end{aligned} \tag{21}$$

are straightforwardly derived from the first-order approximation model. In TBT, no shear correction coefficient is considered, since it depends upon several parameters, such as the geometry of the cross-section (see, for instance, Cowper [16] and Murty [17]). Higher-order models yield a more detailed description of the shear mechanics (no shear correction coefficient is required), of the

in- and out-of-section deformations, of the coupling of the spatial directions due to Poisson's effect and of the torsional mechanics than classical models do. EBT theory neglects them all, since it was formulated to describe a pure bending mechanics. TBT model accounts for constant shear stress and strain components. In the case of classical models, the material stiffness coefficients should be corrected in order to contrast a phenomenon known in literature as Poisson's locking (see Giunta et al. [18]).

4. Governing equations

The governing equations and the boundary conditions are derived through the PVD:

$$\delta L_i = 0 \tag{22}$$

where δ stands for a virtual variation and L_i represents the strain energy. According to the grouping of the stress and strain components in Eqs. (2) and (3), the virtual variation of the strain energy for a thermo-mechanical case is:

$$\delta L_i = \int_l \int_\Omega \left[\delta \boldsymbol{\epsilon}_n^T (\boldsymbol{\sigma}_{ne} - \boldsymbol{\sigma}_{nt}) + \delta \boldsymbol{\epsilon}_p^T (\boldsymbol{\sigma}_{pe} - \boldsymbol{\sigma}_{pt}) \right] d\Omega \, dx \tag{23}$$

By substitution of the geometrical relations, Eq. (5), the constitutive equations, Eq. (7), and the unified hierarchical approximation of the displacements, Eq. (17), Eq. (23) becomes:

$$\begin{aligned}
\delta L_i = & \int_l \delta \mathbf{u}_\tau^T \int_\Omega \Big[(\mathbf{D}_{np} F_\tau)^T \mathbf{C}_{np} (\mathbf{D}_p F_s) + (\mathbf{D}_{np} F_\tau)^T \mathbf{C}_{nn} (\mathbf{D}_{np} F_s) \\
& + (\mathbf{D}_{np} F_\tau)^T \mathbf{C}_{nn} F_s \mathbf{D}_{nx} + (\mathbf{D}_p F_\tau)^T \mathbf{C}_{pp} (\mathbf{D}_p F_s) + (\mathbf{D}_p F_\tau)^T \mathbf{C}_{pn} (\mathbf{D}_{np} F_s) \\
& + (\mathbf{D}_p F_\tau)^T \mathbf{C}_{pn} F_s \mathbf{D}_{nx} + \mathbf{D}_{nx}^T \mathbf{C}_{np} F_\tau (\mathbf{D}_p F_s) \\
& + \mathbf{D}_{nx}^T \mathbf{C}_{nn} F_\tau (\mathbf{D}_{np} F_s) + \mathbf{D}_{nx}^T \mathbf{C}_{nn} F_\tau F_s \mathbf{D}_{nx} \Big] d\Omega \, \mathbf{u}_s \, dx \\
& - \int_l \delta \mathbf{u}_\tau^T \int_\Omega \Big[(\mathbf{D}_{np} F_\tau)^T (\lambda_n \Theta_\Omega \mathbf{I}) + (\mathbf{D}_p F_\tau)^T (\lambda_p \Theta_\Omega \mathbf{I}) \\
& + \mathbf{D}_{nx}^T F_\tau (\lambda_n \Theta_\Omega \mathbf{I}) \Big] d\Omega \, \Theta_n \, dx
\end{aligned} \tag{24}$$

After integration by parts, Eq. (24) reads:

$$\begin{aligned}
\delta L_i = & \int_l \delta \mathbf{u}_\tau^T \int_\Omega \Big[(\mathbf{D}_{np} F_\tau)^T \mathbf{C}_{np} (\mathbf{D}_p F_s) + (\mathbf{D}_{np} F_\tau)^T \mathbf{C}_{nn} (\mathbf{D}_{np} F_s) \\
& + (\mathbf{D}_{np} F_\tau)^T \mathbf{C}_{nn} F_s \mathbf{D}_{nx} + (\mathbf{D}_p F_\tau)^T \mathbf{C}_{pp} (\mathbf{D}_p F_s) + (\mathbf{D}_p F_\tau)^T \mathbf{C}_{pn} (\mathbf{D}_{np} F_s) \\
& + (\mathbf{D}_p F_\tau)^T \mathbf{C}_{pn} F_s \mathbf{D}_{nx} - \mathbf{D}_{nx}^T \mathbf{C}_{np} F_\tau (\mathbf{D}_p F_s) - \mathbf{D}_{nx}^T \mathbf{C}_{nn} F_\tau (\mathbf{D}_{np} F_s) \\
& - \mathbf{D}_{nx}^T \mathbf{C}_{nn} F_\tau F_s \mathbf{D}_{nx} \Big] d\Omega \, \mathbf{u}_s \, dx - \int_l \delta \mathbf{u}_\tau^T \int_\Omega \Big[(\mathbf{D}_{np} F_\tau)^T (\lambda_n \Theta_\Omega \mathbf{I}) \\
& + (\mathbf{D}_p F_\tau)^T (\lambda_p \Theta_\Omega \mathbf{I}) - \mathbf{D}_{nx}^T F_\tau (\lambda_n \Theta_\Omega \mathbf{I}) \Big] d\Omega \, \Theta_n \, dx \\
& + \delta \mathbf{u}_\tau^T \int_\Omega F_\tau \left[\mathbf{C}_{np} (\mathbf{D}_p F_s) + \mathbf{C}_{nn} (\mathbf{D}_{np} F_s) + \mathbf{C}_{nn} F_s \mathbf{D}_{nx} \right] d\Omega \, \mathbf{u}_s \Big|_{x=0}^{x=l} \\
& - \delta \mathbf{u}_\tau^T \int_\Omega F_\tau (\lambda_n \Theta_\Omega \mathbf{I}) d\Omega \, \Theta_n \Big|_{x=0}^{x=l}
\end{aligned} \tag{25}$$

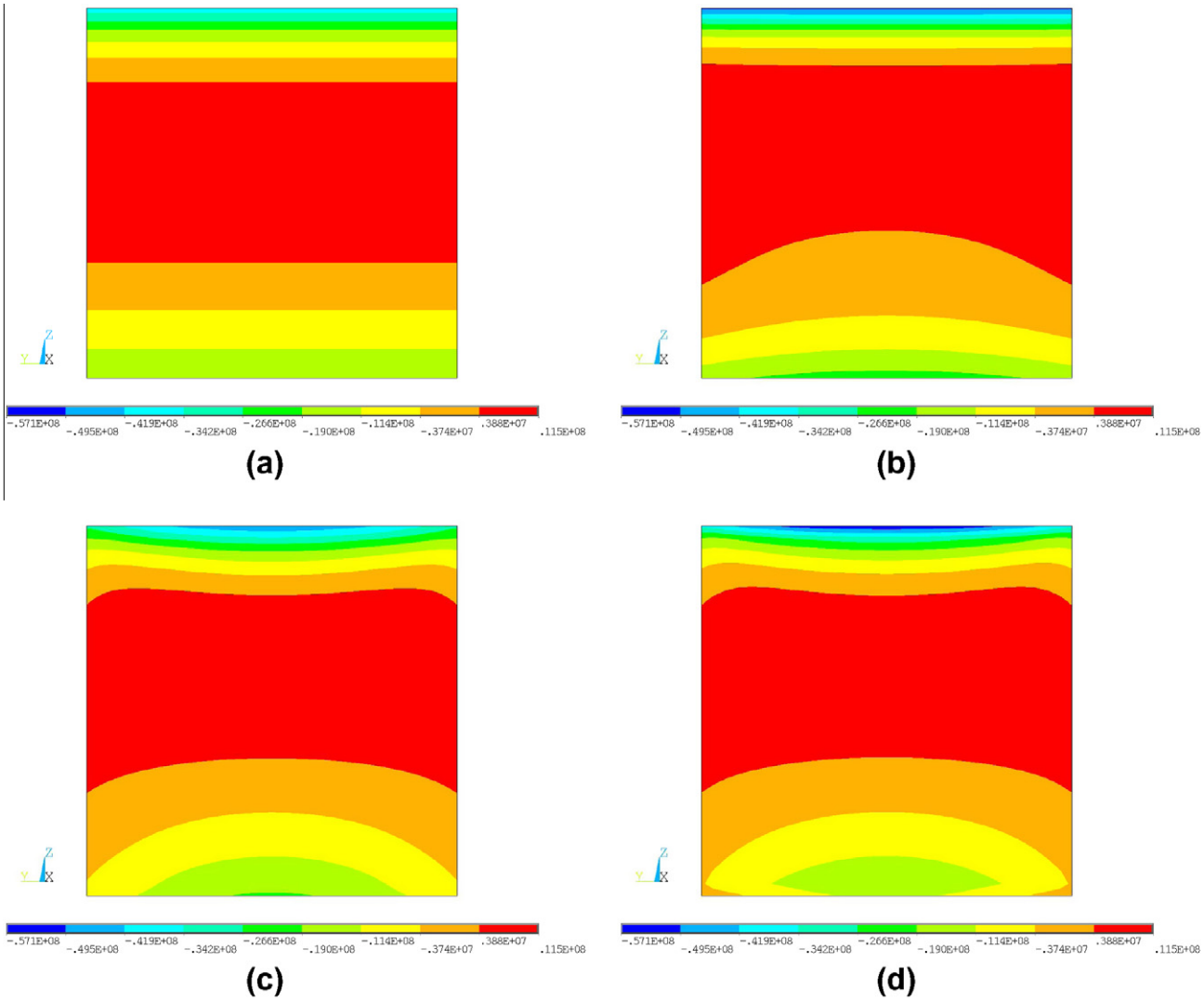

Fig. 7. Mono-layer FGM beam, σ_{xx} [Pa] at $x/l = 1/2$ via (a) TBT, (b) $N = 4$, (c) $N = 13$ and (d) FEM 3D^a, $l/a = 10$.

In a compact vectorial form:

$$\delta L_i = \int_l \delta \mathbf{u}_\tau^T \overline{\mathbf{K}}_{uu}^{\tau s} \mathbf{u}_s \, dx - \int_l \delta \mathbf{u}_\tau^T \overline{\mathbf{K}}_{u\theta}^{\tau} \Theta_n \, dx + \left[\delta \mathbf{u}_\tau^T \overline{\mathbf{\Pi}}_{uu}^{\tau s} \mathbf{u}_s\right]_{x=0}^{x=l} - \left[\delta \mathbf{u}_\tau^T \overline{\mathbf{\Pi}}_{u\theta}^{\tau} \Theta_n\right]_{x=0}^{x=l} \tag{26}$$

The components of the differential stiffness matrix $\overline{\mathbf{K}}_{uu}^{\tau s}$ are:

$$\begin{aligned}
&\overline{K}_{uu_{xx}}^{\tau s} = J_{\tau,y s,y}^{66} + J_{\tau,z s,z}^{55} - J_{\tau s}^{11} \frac{\partial^2}{\partial x^2} \quad \overline{K}_{uu_{xy}}^{\tau s} = \left(J_{\tau,y s}^{66} - J_{\tau s,y}^{12}\right) \frac{\partial}{\partial x} \\
&\overline{K}_{uu_{xz}}^{\tau s} = \left(J_{\tau,z s}^{55} - J_{\tau s,z}^{13}\right) \frac{\partial}{\partial x} \\
&\overline{K}_{uu_{yy}}^{\tau s} = J_{\tau,y s,y}^{22} + J_{\tau,z s,z}^{44} - J_{\tau s}^{66} \frac{\partial^2}{\partial x^2} \quad \overline{K}_{uu_{yx}}^{\tau s} = \left(J_{\tau,y s}^{12} - J_{\tau s,y}^{66}\right) \frac{\partial}{\partial x} \\
&\overline{K}_{uu_{yz}}^{\tau s} = J_{\tau,y s,z}^{23} + J_{\tau,z s,y}^{44} \\
&\overline{K}_{uu_{zz}}^{\tau s} = J_{\tau,y s,y}^{44} + J_{\tau,z s,z}^{33} - J_{\tau s}^{55} \frac{\partial^2}{\partial x^2} \quad \overline{K}_{uu_{zx}}^{\tau s} = \left(J_{\tau,z s}^{13} - J_{\tau s,z}^{55}\right) \frac{\partial}{\partial x} \\
&\overline{K}_{uu_{zy}}^{\tau s} = J_{\tau,z s,y}^{23} + J_{\tau,y s,z}^{44}
\end{aligned} \tag{27}$$

The generic term $J_{\tau_{(,\phi)} s_{(,\xi)}}^{gh}$ is a cross-section moment:

$$J_{\tau_{(,\phi)} s_{(,\xi)}}^{gh} = \int_\Omega C_{gh} F_{\tau_{(,\phi)}} F_{s_{(,\xi)}} \, d\Omega \tag{28}$$

The components of the differential thermo-mechanical coupling matrix $\overline{\mathbf{K}}_{u\theta}^{\tau}$ are:

$$\overline{K}_{u\theta_{xx}}^{\tau} = -J_\tau^1 \frac{\partial}{\partial x} \quad \overline{K}_{u\theta_{yy}}^{\tau} = J_{\tau,y}^2 \quad \overline{K}_{u\theta_{zz}}^{\tau} = J_{\tau,z}^3 \tag{29}$$

The generic term $J_{\tau_{(,\phi)}}^{g}$ is:

$$J_{\tau_{(,\phi)}}^{g} = \int_\Omega F_{\tau_{(,\phi)}} \lambda_g \Theta_\Omega \, d\Omega \tag{30}$$

As far as the boundary conditions are concerned, the components of $\overline{\mathbf{\Pi}}_{uu}^{\tau s}$ are:

$$\begin{aligned}
&\overline{\Pi}_{uu_{xx}}^{\tau s} = J_{\tau s}^{11} \frac{\partial}{\partial x} \quad \overline{\Pi}_{uu_{xy}}^{\tau s} = J_{\tau s,y}^{12} \quad \overline{\Pi}_{uu_{xz}}^{\tau s} = J_{\tau s,z}^{13} \\
&\overline{\Pi}_{uu_{yy}}^{\tau s} = J_{\tau s}^{66} \frac{\partial}{\partial x} \quad \overline{\Pi}_{uu_{yx}}^{\tau s} = J_{\tau s,y}^{66} \quad \overline{\Pi}_{uu_{yz}}^{\tau s} = 0 \\
&\overline{\Pi}_{uu_{zz}}^{\tau s} = J_{\tau s}^{55} \frac{\partial}{\partial x} \quad \overline{\Pi}_{uu_{zx}}^{\tau s} = J_{\tau s,z}^{55} \quad \overline{\Pi}_{uu_{zy}}^{\tau s} = 0
\end{aligned} \tag{31}$$

and the components of $\overline{\mathbf{\Pi}}_{u\theta}^{\tau}$ are:

$$\overline{\Pi}_{u\theta_{xx}}^{\tau} = J_\tau^1 \quad \overline{\Pi}_{u\theta_{yy}}^{\tau} = 0 \quad \overline{\Pi}_{u\theta_{zz}}^{\tau} = 0 \tag{32}$$

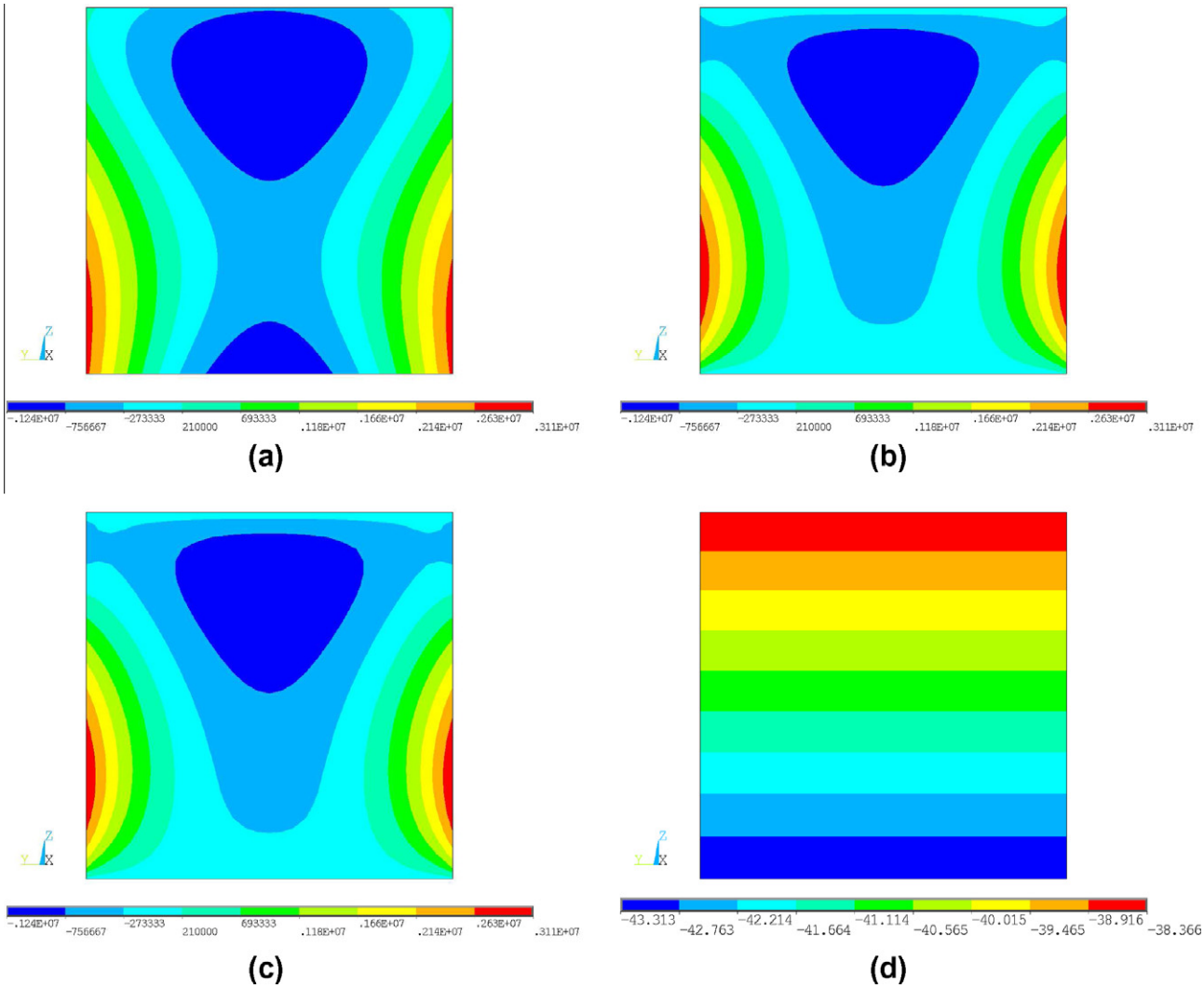

Fig. 8. Mono-layer FGM beam, σ_{xz} [Pa] at $x/l = 0$ via (a) $N = 4$, (b) $N = 13$, (c) FEM 3D[a] and (d) TBT, $l/a = 10$.

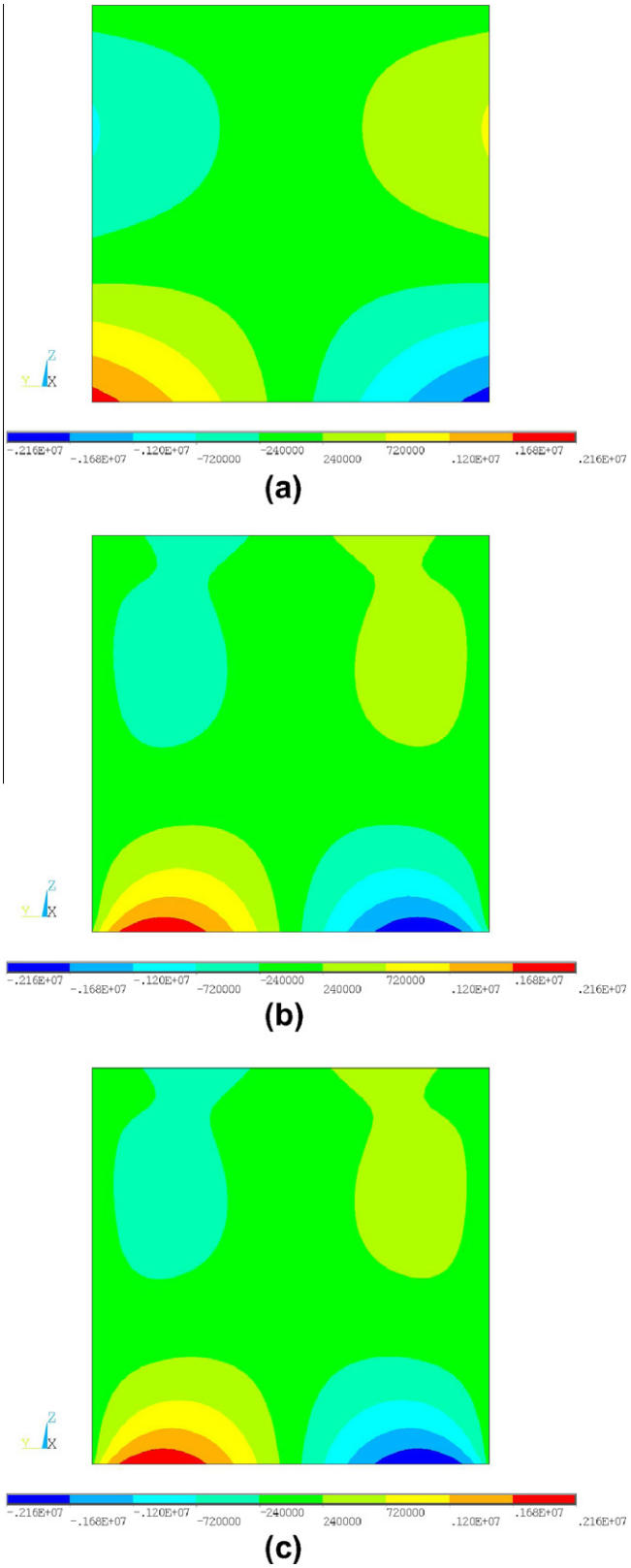

Fig. 9. Mono-layer FGM beam, σ_{xy} [Pa] at $x/l = 0$ via (a) $N = 4$, (b) $N = 13$ and (c) FEM 3D^a, $l/a = 10$.

The fundamental nucleo of the governing equations in a compact vectorial form is:

$$\delta \mathbf{u}_\tau^T : \quad \overline{\mathbf{K}}_{uu}^{\tau s} \mathbf{u}_s = \overline{\mathbf{K}}_{u\theta}^{\tau} \Theta_n \tag{33}$$

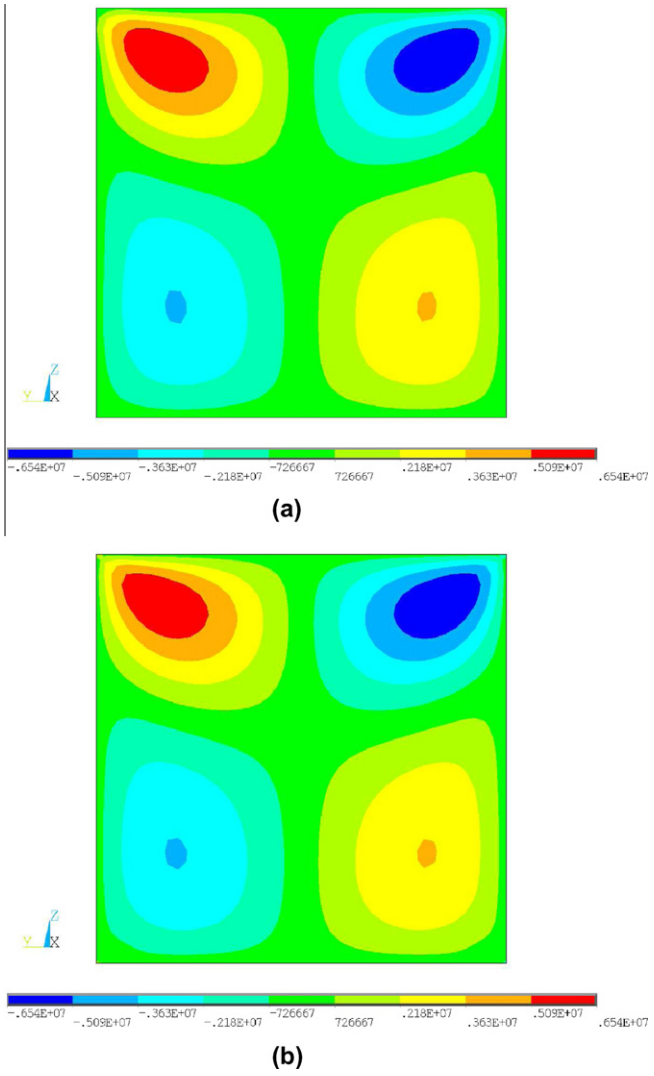

Fig. 10. Mono-layer FGM beam, σ_{yz} [Pa] at $x/l = 1/2$ via (a) $N = 13$ and (b) FEM 3D^a, $l/a = 10$.

In explicit form:

$$\begin{aligned}
\delta u_{x\tau} : & -J_{\tau s}^{11} u_{xs,xx} + \left(J_{\tau,zs,z}^{55} + J_{\tau,ys,y}^{66}\right) u_{xs} + \left(J_{\tau,ys}^{66} - J_{\tau s,y}^{12}\right) u_{ys,x} \\
& + \left(J_{\tau,zs}^{55} - J_{\tau s,z}^{13}\right) u_{zs,x} = -J_{\tau}^{1} \Theta_{n,x} \\
\delta u_{y\tau} : & \left(J_{\tau,ys}^{12} - J_{\tau s,y}^{66}\right) u_{xs,x} - J_{\tau s}^{66} u_{ys,xx} + \left(J_{\tau,ys,y}^{22} + J_{\tau,zs,z}^{44}\right) u_{ys} \\
& + + \left(J_{\tau,ys,z}^{23} + J_{\tau,zs,y}^{44}\right) u_{zs} = J_{\tau,y}^{2} \Theta_n \\
\delta u_{z\tau} : & \left(J_{\tau,zs}^{13} - J_{\tau s,z}^{55}\right) u_{xs,x} + \left(J_{\tau,zs,y}^{23} + J_{\tau,ys,z}^{44}\right) u_{ys} - J_{\tau s}^{55} u_{zs,xx} \\
& + + \left(J_{\tau,zs,z}^{33} + J_{\tau,ys,y}^{44}\right) u_{zs} = J_{\tau,z}^{3} \Theta_n
\end{aligned} \tag{34}$$

The fundamental nucleo of the natural and mechanical boundary conditions at $x = 0$ and l are:

$$\begin{aligned}
& \text{either } u_{x\tau} = \bar{u}_{x\tau} \quad \text{or} \quad J_{\tau s}^{11} u_{xs,x} + J_{\tau s,y}^{12} u_{ys} + J_{\tau s,z}^{13} u_{zs} - J_{\tau}^{1} \Theta_n = 0 \\
& \text{either } u_{y\tau} = \bar{u}_{y\tau} \quad \text{or} \quad J_{\tau s,y}^{66} u_{xs} + J_{\tau s}^{66} u_{ys,x} = 0 \\
& \text{either } u_{z\tau} = \bar{u}_{z\tau} \quad \text{or} \quad J_{\tau s,z}^{55} u_{xs} + J_{\tau s}^{55} u_{zs,x} = 0
\end{aligned} \tag{35}$$

For a fixed approximation order, the nucleo has to be expanded versus the indexes τ and s in order to obtain the governing equations and the boundary conditions of the desired model.

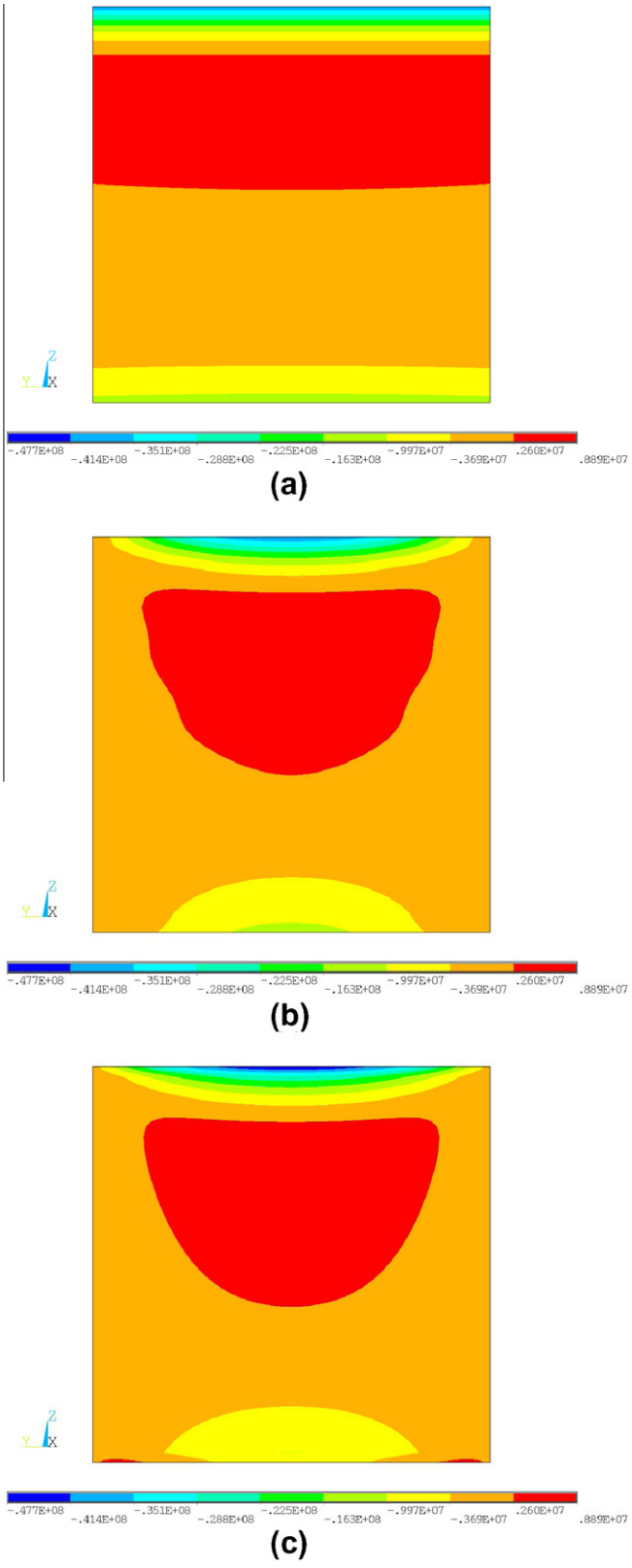

Fig. 11. Mono-layer FGM beam, σ_{yy} [Pa] at $x/l = 1/2$ via (a) $N = 4$, (b) $N = 13$ and (c) FEM 3D[a], $l/a = 10$.

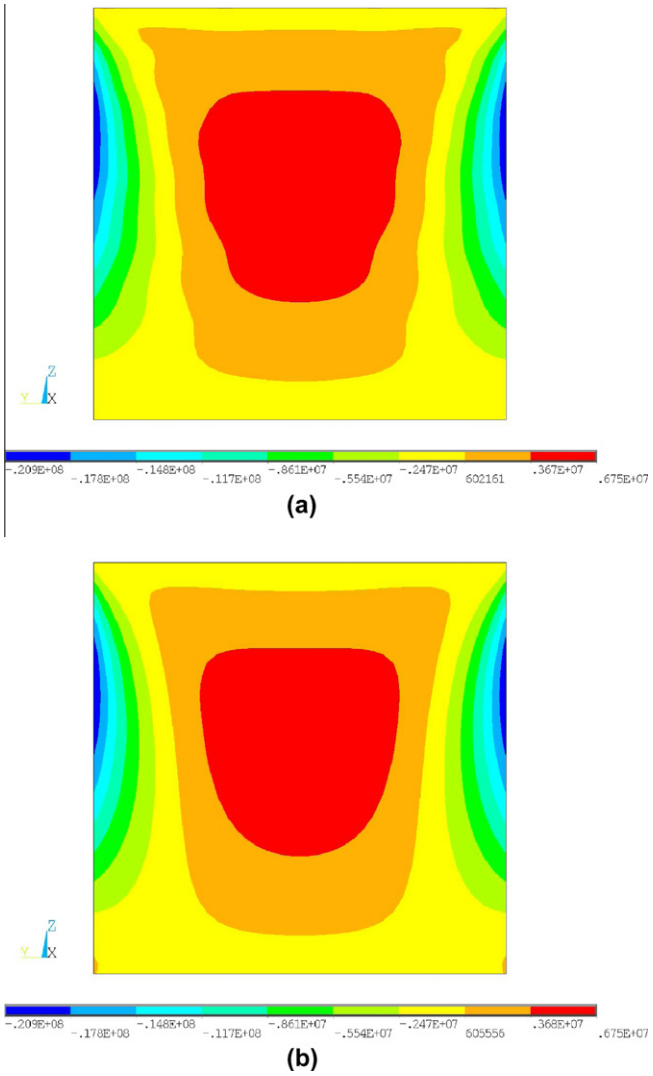

Fig. 12. Mono-layer FGM beam, σ_{zz} [Pa] at $x/l = 1/2$ via (a) $N = 13$ and (b) FEM 3D[a], $l/a = 10$.

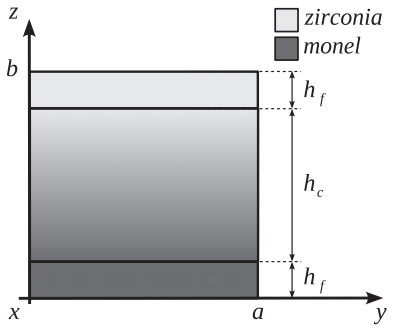

Fig. 13. Sandwich FGM beam.

5. Closed form analytical solution

The differential equations are solved via a Navier-type solution. Simply supported beams are, therefore, investigated. The following harmonic form for the axial variation of the displacement and temperature fields is adopted:

$$\begin{aligned} u_x &= U_{x\tau} F_\tau(y,z)\cos(\alpha x) \\ u_y &= U_{y\tau} F_\tau(y,z)\sin(\alpha x) \\ u_z &= U_{z\tau} F_\tau(y,z)\sin(\alpha x) \\ T &= \Theta_\Omega(y,z)\Theta_n(x) = \Theta_\Omega \sin(\alpha x) \end{aligned} \tag{36}$$

Table 7
Sandwich FGM beam, displacements [m], $l/a = 100$.

	$-1 \cdot u_z$	$-10 \cdot u_x$	$10^3 \cdot u_y$
FEM 3D[a]	1.022	1.126	1.919
FEM 3D[b]	1.019	1.127	1.902
$N = 11 - 13$	1.023	1.126	1.900
$N = 9,10$	1.023	1.126	1.899
$N = 8$	1.023	1.126	1.898
$N = 7$	1.023	1.126	1.890
$N = 6$	1.024	1.126	1.883
$N = 5$	1.024	1.126	1.868
$N = 4$	1.024	1.126	1.865
$N = 3$	1.024	1.126	1.827
$N = 2$	1.047	1.122	1.763
TBT, EBT	1.021	1.126	0.000

[a] Mesh $30 \times 30 \times 30$.
[b] Mesh $20 \times 20 \times 20$.

Table 8
Sandwich FGM beam, stresses [Pa], $l/a = 100$.

	$10^{-7} \cdot \sigma_{xx}$	$10^{-5} \cdot \sigma_{xz}$	$10^{-6} \cdot \sigma_{zz}$
FEM 3D[a]	1.457	3.881	7.721
FEM 3D[b]	1.460	3.871	7.737
$N = 13$	1.465	3.870	7.828
$N = 12$	1.462	3.883	7.739
$N = 11$	1.449	3.911	7.479
$N = 10$	1.444	3.919	7.416
$N = 9$	1.463	3.912	7.811
$N = 8$	1.487	3.852	8.293
$N = 7$	1.502	3.749	8.528
$N = 6$	1.533	3.883	8.843
$N = 5$	1.422	3.826	6.777
$N = 4$	1.036	3.285	−0.090
$N = 3$	1.300	3.721	3.897
$N = 2$	3.118	2.459	31.22
TBT	1.037	4.869[c]	–[d]
EBT	1.032	–	–

[a] Mesh $30 \times 30 \times 30$.
[b] Mesh $20 \times 20 \times 20$.
[c] Scaling factor -10^5 (instead of 10^{-5}).
[d] Result not provided by the theory.

Table 9
Sandwich FGM beam, displacements [m], $l/a = 10$.

	$-10^2 \cdot u_z$	$-10^2 \cdot u_x$	$10^3 \cdot u_y$
FEM 3D[a]	1.033	1.118	1.894
FEM 3D[b]	1.029	1.119	1.895
$N = 12,13$	1.034	1.118	1.894
$N = 10,11$	1.034	1.118	1.893
$N = 8,9$	1.034	1.118	1.892
$N = 7$	1.034	1.118	1.883
$N = 6$	1.034	1.118	1.877
$N = 5$	1.033	1.118	1.861
$N = 4$	1.034	1.118	1.858
$N = 3$	1.034	1.118	1.818
$N = 2$	1.063	1.114	1.741
TBT	1.033	1.113	0.000
EBT	1.033	1.112	0.000

[a] Mesh $30 \times 30 \times 30$.
[b] Mesh $20 \times 20 \times 20$.

where α is:

$$\alpha = \frac{m\pi}{l} \tag{37}$$

$m \in \mathbf{N}^+$ represents the half-wave number along the beam axis. $\{U_{i\tau}: i = x,y,z\}$ are the maximal amplitudes of the displacement components. Upon substitution of Eq. (36) into Eq. (34), the algebraic fundamental nucleo is obtained:

$$\begin{aligned}
\delta U_{x\tau} &: \left(\alpha^2 J^{11}_{\tau s} + J^{55}_{\tau_{,z} s_{,z}} + J^{66}_{\tau_{,y} s_{,y}}\right) U_{xs} + \alpha\left(J^{66}_{\tau_{,y} s} - J^{12}_{\tau s_{,y}}\right) U_{ys} \\
&\quad + \alpha\left(J^{55}_{\tau_{,z} s} - J^{13}_{\tau s_{,z}}\right) U_{zs} = -\alpha J^1_{\tau} \\
\delta U_{y\tau} &: \alpha\left(J^{66}_{\tau s_{,y}} - J^{12}_{\tau_{,y} s}\right) U_{xs} + \left(\alpha^2 J^{66}_{\tau s} + J^{22}_{\tau_{,y} s_{,y}} + J^{44}_{\tau_{,z} s_{,z}}\right) U_{ys} \\
&\quad + \left(J^{23}_{\tau_{,y} s_{,z}} + J^{44}_{\tau_{,z} s_{,y}}\right) U_{zs} = J^2_{\tau_{,y}} \\
\delta U_{z\tau} &: \alpha\left(J^{55}_{\tau s_{,z}} - J^{13}_{\tau_{,z} s}\right) U_{xs} + \left(J^{23}_{\tau_{,z} s_{,y}} + J^{44}_{\tau_{,y} s_{,z}}\right) U_{ys} \\
&\quad + \left(\alpha^2 J^{55}_{\tau s} + J^{33}_{\tau_{,z} s_{,z}} + J^{44}_{\tau_{,y} s_{,y}}\right) U_{zs} = J^3_{\tau_{,z}}
\end{aligned} \tag{38}$$

The determination of the temperature profile by solving Fourier's heat conduction equation is presented in Appendix A.

Table 10
Sandwich FGM beam, stresses [Pa], $l/a = 10$.

	$10^{-7} \cdot \sigma_{xx}$	$10^{-6} \cdot \sigma_{xz}$	$10^{-6} \cdot \sigma_{zz}$
FEM 3D[a]	1.237	3.921	8.701
FEM 3D[b]	1.239	3.910	8.721
$N = 13$	1.245	3.910	8.802
$N = 12$	1.242	3.922	8.700
$N = 11$	1.229	3.951	8.441
$N = 10$	1.222	3.959	8.358
$N = 9$	1.242	3.951	8.757
$N = 8$	1.269	3.891	9.29
$N = 7$	1.284	3.785	9.526
$N = 6$	1.317	3.920	9.888
$N = 5$	1.206	3.863	7.790
$N = 4$	0.783	3.311	0.269
$N = 3$	1.053	3.752	4.346
$N = 2$	3.080	2.483	35.13
TBT	1.303	4.816[c]	–[d]
EBT	1.297	–	–

[a] Mesh $30 \times 30 \times 30$.
[b] Mesh $20 \times 20 \times 20$.
[c] Scaling factor -0.1 (instead of 10^{-6}).
[d] Result not provided by the theory.

6. Numerical results and discussion

A ceramic–metallic gradation along the thickness direction is considered. The ceramic phase is made of Zirconia (ZrO_2), whereas Monel (70Ni–30Cu), a nikel-based alloy, is considered as metallic phase. Materials properties are presented in Table 2. The generic material property, f, is assumed to vary versus the thickness coordinate z according to the following power law distribution:

$$f = (f_1 - f_2)(\alpha_z z + \beta_z)^{n_z} + f_2 \tag{39}$$

This law is obtained through the assumption of a power gradation law of the volume fraction of the two constituent materials and the rule of mixtures, see Praveen and Reddy [19] and Chakraborty et al. [3]. n_z is the power law exponent and it is equal to the unit, f_i is the generic material property of each constituent and α_z and β_z are two constant coefficients that depend upon the through-the-thickness extension of the FGM layer and the through-the-thickness position of the center of the reference system, which is centred at the cross-section bottom left corner. A mono-layer and a sandwich FGM cross-section configuration are investigated. In the case of the mono-layer FGM cross-section and for the assumed reference system, $\alpha_z = 1/b$ and $\beta_z = 0$. The half-wave number m in Eq. (37) is equal to one. The thermal boundary conditions (see Eq. (45) in Appendix A) are: $T_t = +400$ K and $T_b = +300$ K. Square cross-sections with sides length $a = b = 1$ m are considered. The length-to-side ratio l/a is equal to

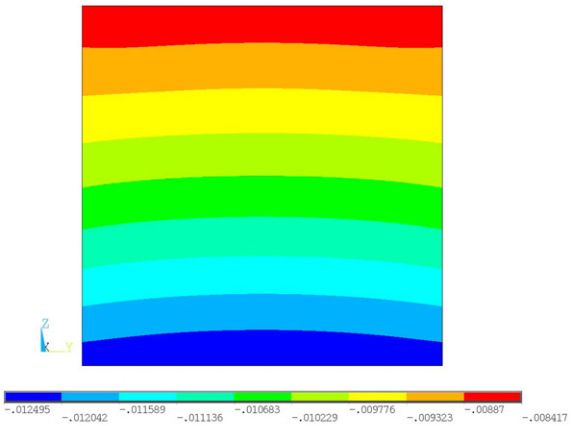

(a) u_z, $N = 13$, $x/l = 1/2$

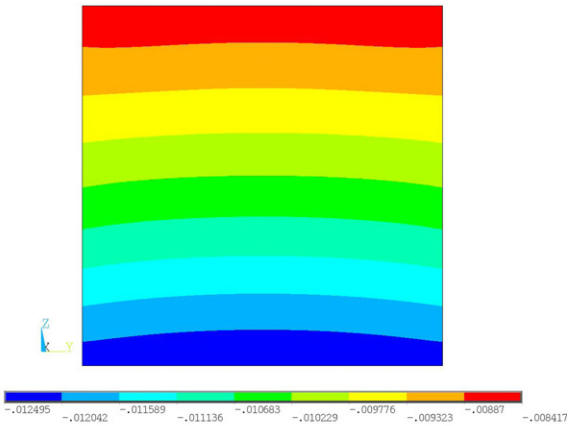

(b) u_z, FEM 3D^a, $x/l = 1/2$

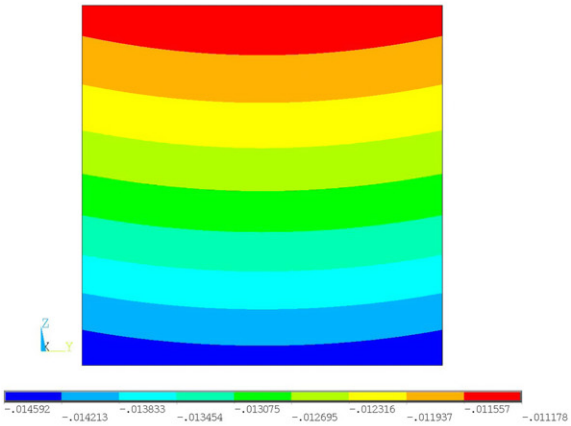

(c) u_x, $N = 13$, $x/l = 0$

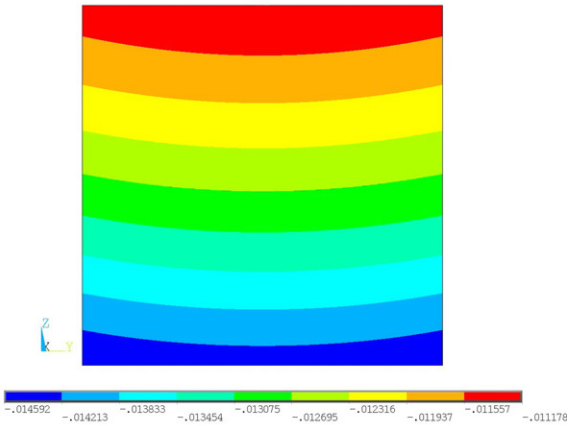

(d) u_x, FEM 3D^a, $x/l = 0$

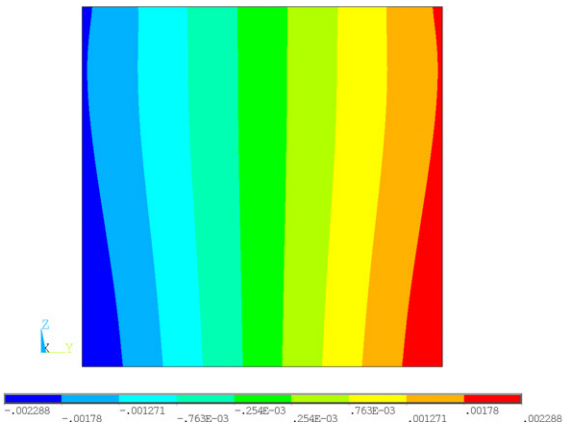

(e) u_y, $N = 13$, $x/l = 1/2$

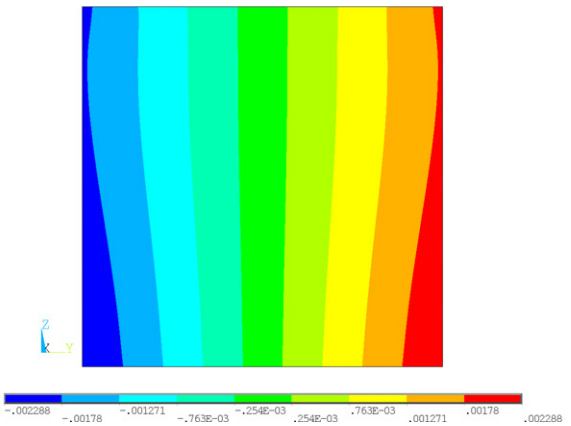

(f) u_y, FEM 3D^a, $x/l = 1/2$

Fig. 14. Sandwich FGM beam, displacements components [m] via $N = 13$ and FEM 3D^a, $l/a = 10$.

100 and 10. Slender and deep beams are, therefore, investigated. As far as tabular results are concerned, the displacements and stresses evaluated at the following points are considered:

$$\bar{u}_x = u_x(0, a/2, b) \quad \bar{u}_y = u_y(l/2, a, b) \quad \bar{u}_z = u_z(l/2, a/2, b/2)$$
$$\bar{\sigma}_{xx} = \sigma_{xx}(l/2, a/2, b/2) \quad \bar{\sigma}_{xz} = \sigma_{xz}(0, 0, b/2) \quad \bar{\sigma}_{zz} = \sigma_{zz}(l/2, a/2, b/2) \tag{40}$$

Results obtained using the proposed higher-order models are compared with three-dimensional FEM solutions obtained via the commercial code ANSYS®. The three-dimensional quadratic element "Solid90" is used for the thermal analysis, whereas the 20-node element "Solid186" is considered for the mechanical problem. For a FGM layer, each element is considered as homogeneous by referring to the material properties at its centre. The accuracy of the three-dimensional FEM solution depends upon both the FEM numerical approximation and the approximation of the gradation law. In order to present the convergence of the three-dimensional reference solution, two different meshes are considered for each analysis. The acronym FEM 3D^a stands for a three-dimensional FEM model with a $30 \times 30 \times 30$ elements mesh,

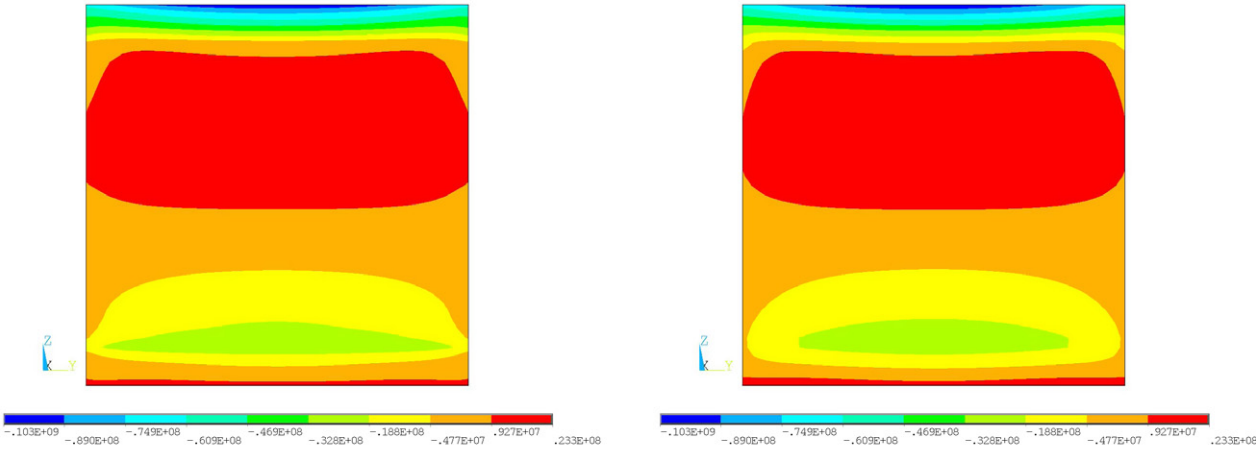

(a) σ_{xx}, $N = 13$, $x/l = 1/2$ (b) σ_{xx}, FEM 3D^a, $x/l = 1/2$

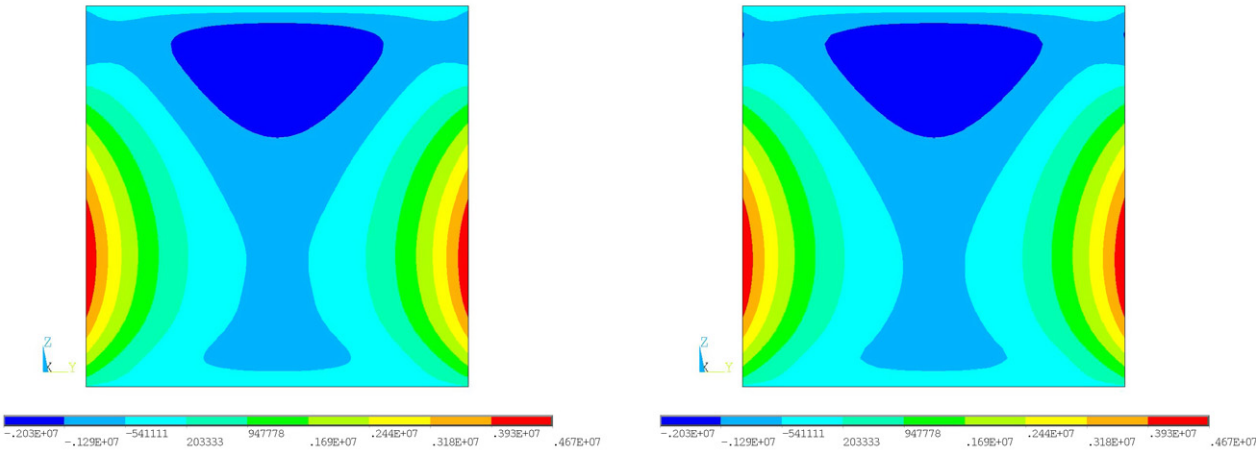

(c) σ_{xz}, $N = 13$, $x/l = 0$ (d) σ_{xz}, FEM 3D^a, $x/l = 0$

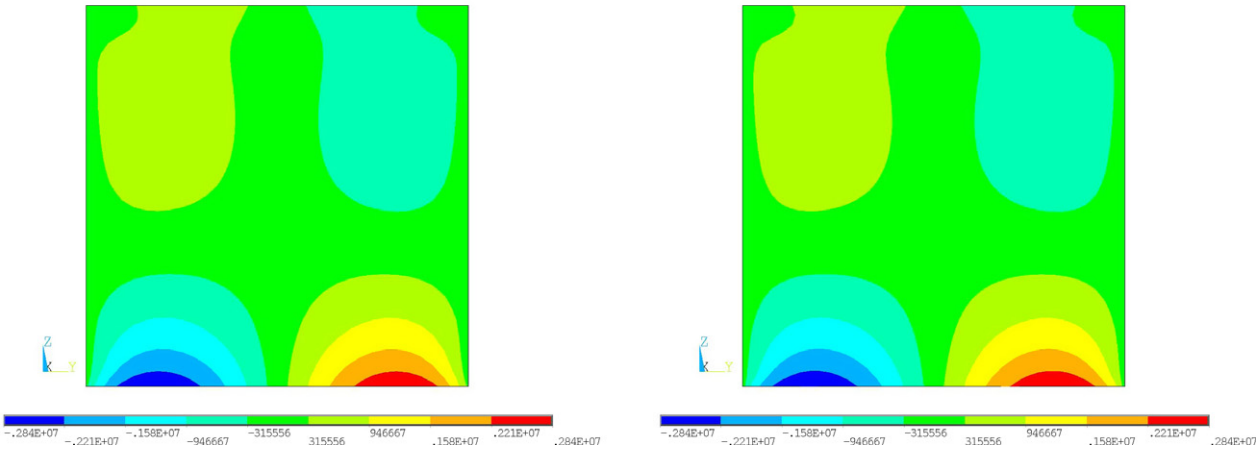

(e) σ_{xy}, $N = 13$, $x/l = 0$ (f) σ_{xy}, FEM 3D^a, $x/l = 0$

Fig. 15. Sandwich FGM beam, $\boldsymbol{\sigma}_n$ stress components [Pa] via $N = 13$ and FEM 3D^a, $l/a = 10$.

whereas the coarser $20 \times 20 \times 20$ mesh solution is addressed by FEM 3D^b. Although the three-dimensional FEM solution and the analytical one are different in nature, some considerations about computational effort can be addressed. The degrees of freedom (DOFs) of the three-dimensional FEM mechanical problem over a beam cross-section as function of the number of elements for each side, n, are $3(3n + 1)(n + 1)$. n is as low as 20 (DOFs = 3843) and as high as 30 (DOFs = 8463). For a fixed approximation order N, the DOFs of the proposed solutions are $3(N + 1)(N + 2)/2$. In the case of the highest considered expansion order ($N = 13$) they are 315.

6.1. Mono-layer FGM beam

Beams made of a single FGM layer, see Fig. 2, are first investigated. The temperature variation over the cross-section at mid-span in presented in Fig. 3. The solution of Fourier's equation via

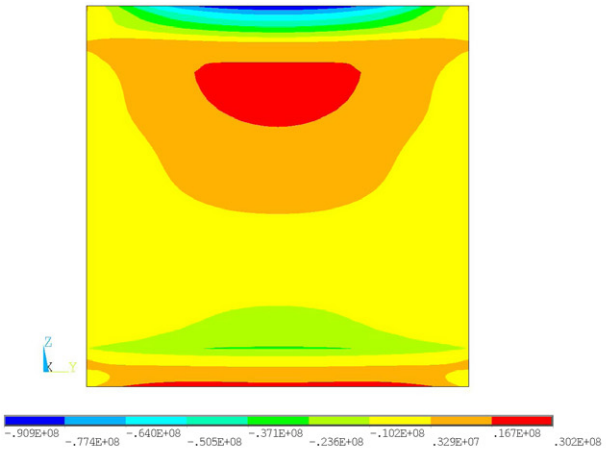

(a) σ_{yy}, $N = 13$

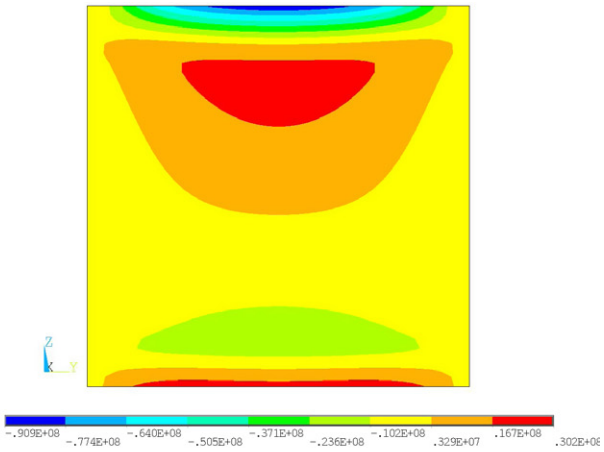

(b) σ_{yy}, FEM 3D^a

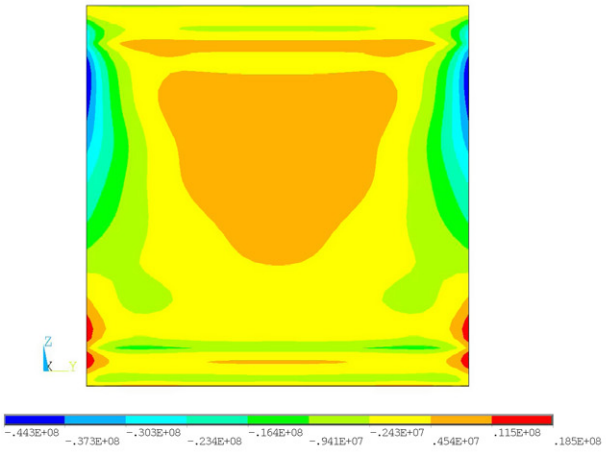

(c) σ_{zz}, $N = 13$

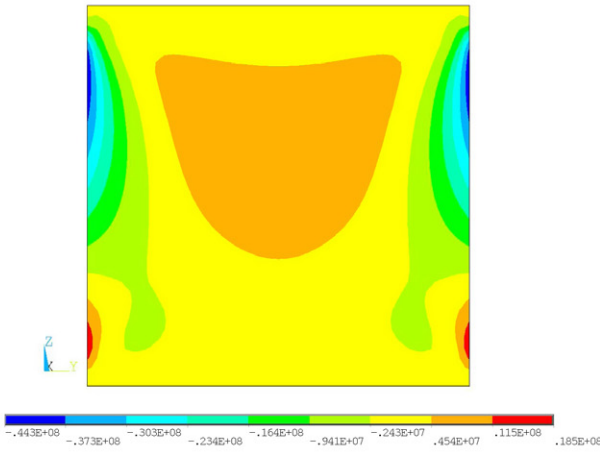

(d) σ_{zz}, FEM 3D^a

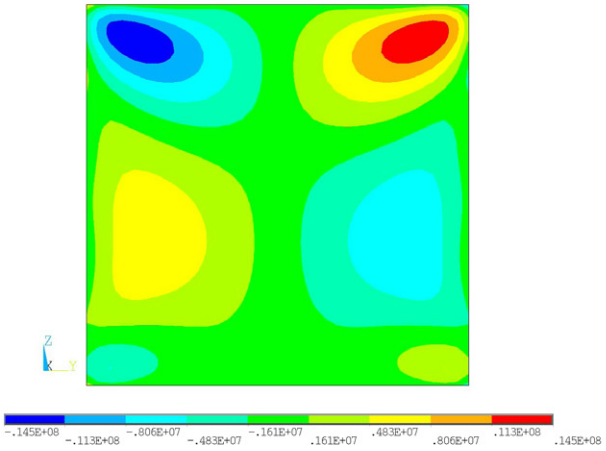

(e) σ_{yz}, $N = 13$

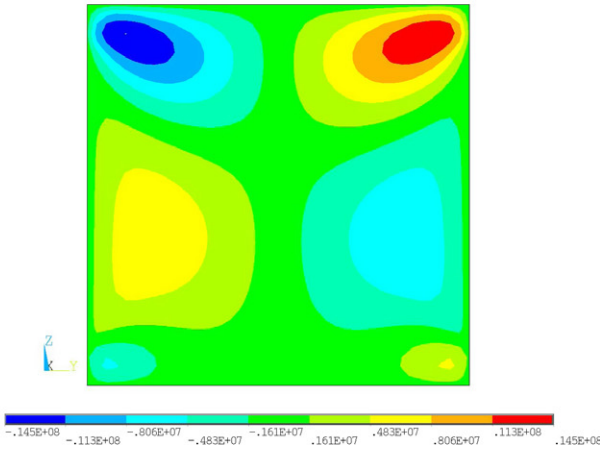

(f) σ_{yz}, FEM 3D^a

Fig. 16. Sandwich FGM beam, $\boldsymbol{\sigma}_n$ stress components [Pa] at $x/l = 1/2$ via $N = 13$ and FEM 3D^a, $l/a = 10$.

the procedure presented in Appendix A has been obtained considering 16 fictitious layers. It matches the FEM 3D^a solution. Tables 3–6 present the displacements and the stresses in Eq. (40) for slender and thick beams. Differently from a bending mechanical load, a thermal load results in axial and through-the-thickness displacement components as well as normal stress components of comparable order of magnitude. This is due to the fact that in the former case the mechanics is mainly governed by bending (and shear, for thick beams), whereas the normal stresses along the other two directions are mainly due to the coupling governed by the Poisson effect. In the thermo-mechanical case, the deformations are governed by the thermal expansion coefficients. Classical theories yield a zero through-the-width displacement since, according to their kinematic hypotheses (see Eqs. (20) and (21)), the

cross-section is rigid on its own plane and the problem is symmetric versus a plane parallel to *Oxz* and passing at mid-width. Nevertheless, they provide a well globally estimated displacement field. As shown in Figs. 4–6, where the variation of the displacement components over the cross-section is presented, lower-order theories match the reference solution FEM 3D[a]. For instance, a fourth-order model is able to predict the trough-the-width variation of the axial displacement component, which it is constant in the case of TBT. As far as the stresses are concerned, higher-order models (e.g., N as low as eight) are required for an accurate solution. The stress field is three-dimensional. Fig. 7 shows the axial stress component at mid-span cross-section. Results are obtained via, TBT, fourth- and 13th-order model and FEM 3D[a]. The latter presents a relevant though-the-width variation and a high through-the-thickness gradient, especially at cross-section top. This is very different from a typical mechanical problem of global bending. The solution for $N = 13$ compares globally well with the reference solution. The shear component σ_{xz} is presented in Fig. 8. TBT yields a solution several order of magnitude smaller than the reference solution. A different scale has been used in the figure and the tables for this reason. A steep stress gradient is present at both cross-section sides. $N = 13$ solution matches the reference one. Fig. 9 presents σ_{xy} computed via $N = 4$ and 13 and FEM 3D[a]. The fourth-order theory yields an acceptable estimation in the neighbourhood of cross-section's centre. The last two solutions compare very well. This is also true for the shear component σ_{yz} presented in Fig. 10. The normal stress component σ_{yy} is shown in Fig. 11. $N = 13$ and FEM 3D[a] solutions compare fairly well. This stress component presents a relevant thought-the-width variation and localised stress zones. A fourth-order approximation is obviously not sufficient to describe it. $N = 13$ yields also a fairly accurate prediction of σ_{zz} as demonstrated by Fig. 12. The results presented in a graphical form have been all obtained for $l/a = 10$. The case of slender beams is very similar and it is not presented here for the sake of brevity.

6.2. Sandwich FGM beam

A FGM sandwich configuration is investigated, see Fig. 13. A FGM core connects the top and bottom layers that are entirely made of zirconia and monel. The thickness, h_f, of the top and bottom faces is 0.1 times the cross-section side length. The solution of Fourier's equation is accurate when compared to the FEM 3D[a] solution. It is not presented here for the sake of brevity. The main difference versus the mono-layer configuration is in a globally slightly cooler bottom part of the cross-section since the ceramic layer acts as a further thermal barrier. Displacements and stresses for slender and thick beams are presented in Tables 7–10. Higher-order models match the reference three-dimensional FEM results. Lower-order and classical theories yield good displacements but are not capable of predicting the stress field properly. When compared with the mono-layer configuration, a higher transverse displacement (resulting in higher stresses) is observed. For the sake of brevity, only a 13th-order model is considered for the plots over the cross-section of displacements and stresses. Fig. 14 shows the displacement components. Results are practically identical. The stress components $\boldsymbol{\sigma}_n$ are presented in Fig. 15. The proposed results and the reference solutions match. The presence of an inner and outer homogeneous layer changes the profile of the axial stress increasing the maximum and minimum values and introducing a stress gradient also at the cross-section bottom. Finally, Fig. 16 presents the stress components $\boldsymbol{\sigma}_p$. The normal stress components also present localised stress areas that make them difficult to be correctly predicted, especially in the case of σ_{zz}. Nevertheless, fairly good results are obtained. A future work perspective consists in a the formulation of higher-order theories by means of a layer-wise approach that should enhance the accuracy of the approximation.

7. Conclusions

A thermo-mechanical analysis of functionally graded beams has been carried out in this paper. Several one-dimensional displacements-based beam models have been derived by means of a unified formulation. Via this formulation, higher-order theories as well as classical Euler–Bernoulli's an Timoshenko's models can be formulated straightforwardly. This is possible thanks a compact notation for the a priori displacement field approximation. A closed form, Navier-type solution has been used. The temperature field has been obtained by solving Fourier's heat conduction equation and it has been accounted for in the mechanical analysis as an external load. Beams made of a single FGM layer as well as a sandwich configurations have been studied. Slender and thick beams have been investigated in terms of temperature, displacements and stresses. Results have been validated through comparison with three-dimensional FEM solutions obtained via the commercial code ANSYS®. In has been shown that the considered thermo-mechanical problems, although presenting a global bending deformation, are governed by three-dimensional stress fields that call for very accurate models. Through an appropriate choice of the approximation order over the cross-section, the proposed formulation yields accurate results with reduced computational costs.

Acknowledgments

The authors would like to sincerely thank the Fonds National de la Recherche (FNR) of Luxembourg for supporting this research via the project FNR CORE C09/MS/05 FUNCTIONALLY and the AFR Grant PHD-MARP-03.

Appendix A

A solution of Fourier's heat conduction equation for FGM beams can be obtained by ideally dividing the cross-section Ω into N_{Ω^k} non-overlapping sub-domains (or layers) along the through-the-thickness direction z:

$$\Omega = \bigcup_{k=1}^{N_{\Omega^k}} \Omega^k \tag{41}$$

Each sub-domain is, then, supposed to be homogeneous, being the elastic and material properties constant and equal to the value at sub-domain's centre. For a kth homogeneous and isotropic layer, the Fourier differential equation becomes:

$$\frac{\partial^2 T^k}{\partial x^2} + \frac{\partial^2 T^k}{\partial y^2} + \frac{\partial^2 T^k}{\partial z^2} = 0 \tag{42}$$

In order to obtain a closed form analytical solution, it is further assumed that the temperature does not depend upon the through-the-width co-ordinate y. This also implies that the material gradation law should be independent from y. The continuity of the temperature and the through-the-thickness heat flux q_z hold at each interface between two consecutive sub-domains:

$$\begin{aligned} T_t^k &= T_b^{k+1} \\ q_{zt}^k &= q_{zb}^{k+1} \end{aligned} \tag{43}$$

Subscript 't' and 'b' stand for sub-domain top and bottom, respectively. The through-the-thickness heat flux is proportional to the temperature derivative versus z:

$$q_z^k = K^k \frac{\partial T^k}{\partial z} \tag{44}$$

being K^k the thermal conductivity. The following temperatures are imposed at cross-section through-the-thickness top and bottom:

$$T = T_t \sin(\alpha x)$$
$$T = T_b \sin(\alpha x) \tag{45}$$

T_t and T_t are the maximal amplitudes and α has been introduced in Eq. (37). The following temperature field:

$$T^k(x,z) = \Theta^k_\Omega(z)\sin(\alpha x) = T^k_0 \exp(sz)\sin(\alpha x) \tag{46}$$

represents a solution of the considered heat conduction problem. T^k_0 is an unknown constant obtained by imposing the boundary condition, whereas s is obtained by replacing Eq. (46) into Eq. (42):

$$s_{1,2} = \pm\alpha \tag{47}$$

$\Theta^k_\Omega(z)$, therefore, becomes:

$$\Theta^k_\Omega(z) = T^k_{01}\exp(+\alpha z) + T^k_{02}\exp(-\alpha z) \tag{48}$$

or, equivalently:

$$\Theta^k_\Omega(z) = C^k_1\cosh(\alpha z) + C^k_2\sinh(\alpha z) \tag{49}$$

For a cross-section division into N_{Ω^k} sub-domains, there are $2\cdot N_{\Omega^k}$ unknowns C^k_j. The problem is mathematically well posed since the boundary conditions in Eqs. (43) and (45) yield a linear algebraic system of $2\cdot N_{\Omega^k}$ equations in C^k_j. The solution convergence versus N_{Ω^k} (although not presented here) has been investigated. It has been found that, for the considered material gradation, $N_{\Omega^k} = 16$ ensures a converged temperature field.

References

[1] Hetnarski RB, Eslami MR. Thermal stresses – advanced theory and applications. Springer; 2009.

[2] Noda N. Thermal stresses in functionally graded materials. J Thermal Stress 1999;22(4–5):477–512.

[3] Chakraborty A, Gopalakrishnan S, Reddy JN. A new beam finite element for the analysis of functionally graded materials. Int J Mech Sci 2003;45(3):519–39.

[4] Carpinteri A, Paggi M. Thermo-elastic mismatch in nonhomogeneous beams. J Eng Math 2008;61(2–4):371–84.

[5] Wang H, Qin Q-H. Meshless approach for thermo-mechanical analysis of functionally graded materials. Eng Anal Bound Elem 2008;32(9):704–12.

[6] Mahi A, Adda Bedia EA, Tounsi A, Mechab I. An analytical method for temperature-dependent free vibration analysis of functionally graded beams with general boundary conditions. Compos Struct 2010;92(8):1877–87.

[7] Wattanasakulpong N, Gangadhara Prusty B, Kelly DW. Thermal buckling and elastic vibration of third-order shear deformable functionally graded beams. Int J Mech Sci 2011;53(9):734–43.

[8] Touloukian YS. Thermophysical properties of high temperature solid materials. New York: MacMillan; 1967.

[9] Brischetto S, Leetsch R, Carrera E, Wallmersperger T, Kröplin B. Thermo-mechanical bending of functionally graded plates. J Thermal Stress 2008;31(3):286–308.

[10] Carrera E. Theories and finite elements for multilayered plates and shells: a unified compact formulation with numerical assessment and benchmarking. Arch Comput Methods Eng 2003;10(3):215–96.

[11] Carrera E, Giunta G, Petrolo M. Beam structures: classical and advanced theories. John Wiley and Sons; 2011.

[12] Giunta G, Belouettar S, Carrera E. Analysis of fgm beams by means of classical and advanced theories. Mech Adv Mater Struct 2010;17(8):622–35.

[13] Giunta G, Crisafulli D, Belouettar S, Carrera E. Hierarchical theories for the free vibration analysis of functionally graded beams. Compos Struct 2011;94(1):68–74.

[14] Catapano A, Giunta G, Belouettar S, Carrera E. Static analysis of laminated beams via a unified formulation. Compos Struct 2011;94(1):75–83.

[15] Philips GM. Interpolation and approximation by polynomials. Springer-Verlag; 2003.

[16] Cowper GR. The shear co-efficient in Timoshenko beam theory. J Appl Mech 1966;33(10):335–40.

[17] Murty AVK. Analysis of short beams. AIAA J 1970;8(11):2098–100.

[18] Giunta G, Biscani F, Belouettar S, Ferreira AJM, Carrera E. Free vibration analysis of composite beams via refined theories. Composite: Part B 2012. http://dx.doi.org/10.1016/j.compositesb.2012.03.005.

[19] Praveen GN, Reddy JN. Nonlinear transient thermoelastic analysis of functionally graded ceramic–metal plates. Int J Solids Struct 1998;35(33):4457–76.